International Journal of Heat and Mass Transfer 65 (2013) 826–844

Contents lists available at SciVerse ScienceDirect

International Journal of Heat and Mass Transfer

journal homepage: www.elsevier.com/locate/ijhmt

Numerical analysis of heat-mass transport and pressure buildup of unsaturated porous medium in a rectangular waveguide subjected to a combined microwave and vacuum system

Khomgris Chaiyo, Phadungsak Rattanadecho *

Research Center of Microwave Utilization in Engineering (R.C.M.E.), Department of Mechanical Engineering, Faculty of Engineering, Thammasat University (Rangsit Campus), Pathumthani 12120, Thailand

ARTICLE INFO

Article history:
Received 13 December 2012
Received in revised form 23 June 2013
Accepted 27 June 2013
Available online 25 July 2013

Keywords:
Microwave
Vacuum
Porous media

ABSTRACT

This paper presents two-dimensional numerical analysis of heat-mass transport and pressure buildup inside an unsaturated porous packed bed which is filled in a rectangular waveguide and subjected to a combined microwave and vacuum system. A microwave system supplies a monochromatic wave in a fundamental TE_{10} mode. The unsaturated porous media is composed of glass beads, water and air. The finite difference time domain method is used to determine the electromagnetic field distribution in the rectangular waveguide by solving the transient Maxwell's equations. The finite difference method together with Newton–Rephson technique is employed to predict the heat, multiphase flow and pressure buildup. The influences of vacuum pressure and operating microwave frequency on temperature, microwave power absorbed, saturation and pressure buildup distribution, and movement of fluid inside the unsaturated porous media are investigated during microwave vacuum drying process.

1. Introduction

Microwave technology has been applied to many drying processes for several decades. In microwave drying, that heat is generated by directly transforming the electromagnetic energy into kinetic energy, thus heat is generated deep within the material to be dried. Some of the successful examples of microwave drying are in a ceramics process for drying and sintering, drying of paper, freeze drying and vulcanization of rubber. Furthermore, excellent reviews of microwave drying are presented by Mujumdar [1], Metaxas and Meridith [2] and Datta and Anantheswaran [3]. In vacuum drying processes can offer reduced drying times and higher end-product quality in comparison with a conventional drying [4–5]. Indeed, operating at low pressure reduces the boiling point of water, and provides low temperature to treat product throughout drying process. Vacuum drying is well known in the metallurgical industries for processing of high purity alloys. It is apparent that microwaves can provide a substantial increase rate of heating in a vacuum environment compared with other methods. However it may be limited not only by the usual restraint of mass transfer but also by the onset breakdown electric filed. Fundamental to the operation of a vacuum drying system is the operating pressure to control the temperature of the product below a prescribed limit.

Fig. 1 shows the boiling point temperature of water versus pressure range of 1–133 kPa (about 0.1–1000 torr). For vacuum drying, the pressure range of 1.33–26.6 kPa (about 10–200 torr) is more successful application to dry heat sensitive materials such as pharmaceutical products and other chemicals. The critical breakdown electric field should be also carefully selected to avoid breakdown electric field responses causing the effect of breakdown in gas such air or water vapor [2].

Microwave vacuum drying provides higher product qualities and an improved drying rate compared to conventional drying processing by experimentally investigated of many researchers. Some of the successful researches of experimental microwave vacuum drying are as followings. Drouzas and Schubert [6] investigated experimentally microwave vacuum dying of banana slices that dehydrated products of excellent quality as examined by taste, color, aroma, smell and rehydration tests compared to conventional drying. Drouzas et al. [7] used a laboratory microwave vacuum drier to investigate drying kinetics experiments with model fruit gel, simulating orange juice concentrate that drying rate constant of the thin-layer drying model is increased with increasing microwave power output and decreasing absolute pressure in vacuum drying. Péré and Rodie [8] presented experimental results obtained by microwave vacuum drying of a packing of initially water saturated glass beads and a packing of initially unsaturated pharmaceutical granules. Sunjka et al. [9] investigated two drying methods of cranberries such microwave-vacuum and

* Corresponding author. Tel.: +66 2564 30019x3153; fax: +66 2564 3010.
E-mail address: ratphadu@engr.tu.ac.th (P. Rattanadecho).

0017-9310/$ - see front matter © 2013 Elsevier Ltd. All rights reserved.
http://dx.doi.org/10.1016/j.ijheatmasstransfer.2013.06.066

Nomenclatures

C	velocity of light (m/s)
C_p	specific heat capacity (J/kg K)
D	binary mass diffusion (m^2/s)
D_m	effective molecular mass diffusion (m^2/s)
E	electromagnetic field intensity (V/m)
f	frequency of the microwave (Hz)
g	gravitational constant (m/s^2)
H_v	specific heat of evaporation (J/kg)
h_c	Heat transfer coefficient (W/m^2 K)
h_m	mass transfer coefficient (m/s)
J	Leverett functions
K	permeability (m^2)
M	molecular weight (kg/mol)
$\dot{n}$	phase change term (kg/m^3 s)
P	microwave power (W)
p	pressure (Pa)
p_{vs}	partial pressure of the saturation vapor (Pa)
Q	microwave power absorbed term (W/m^3)
R	universal gas constant (J/mol K)
S	water saturation
S_e	effective water saturation
S_{ir}	irreducible water saturation
T	temperature (°C)
t	time (s)
u, w	velocity (m/s)

Greek letters

α	attenuation constant
tan δ	loss tangent coefficient
δ_s	skin depth
ε	complex permittivity (F/m)
ε'	permittivity or dielectric constant
ε''	dielectric loss factor
ϕ	porosity
λ_{eff}	effective thermal conductivity (W/m K)
μ	magnetic permeability (H/m) or Dynamic viscosity (Pa s)
ρ	density (kg/m^3)
σ	gas–liquid interfacial tension

Subscripts

0	free space
a	air
c	capillary
g	gas
l	liquid
p	particle
r	relative
v	water vapor
x, z	Cartesian coordinate

microwave-convective that microwave vacuum drying exhibited to enhance characteristics in almost all observed parameters (color, textural characteristics, organoleptic properties) and was more energy-efficient when compared to microwave-convective drying. Hu et al. [10] compared the characteristics of hot air and microwave vacuum combination drying using edamame as the raw material, it was found that combined hot air and microwave vacuum is enable to increase drying rate and enhance product quality.

In a theoretical analysis of heat and mass transfer in porous materials has been studied for several decades and it can be classified into three difference fundamentals as following details.

(1) The single variable model: one diffusion equation of moisture content is used for simple configuration.
(2) The two variables model: two dependent variables as temperature and moisture content are employed, and effect of pressure buildup can be neglected.
(3) The three variables model: three dependent variables as temperature, moisture content, and pressure buildup are used; this model provides better transport phenomena details than other models.

The single variable and two variables model are mostly applied to investigate for a conventional drying because they are not complicated to manipulate numerical scheme. However, a few studies used the three variables model are Datta and Anantheswaran [3], Perré and Turner [11], Rattanadecho [12], and Ni et al. [13].

A few of researchers have numerically studied heat and mass transport phenomena of porous material under microwave drying processing, and most previous works have not mentioned pressure buildup within porous material [14–19]. Some of previous researches [20–21] revealed pressure buildup by using the three variables model for microwave drying of an unsaturated porous media. However, the studies in case of numerically microwave vacuum drying of unsaturated porous material in a rectangular waveguide of a microwave system supplies a monochromatic wave in a fundamental mode (TE_{10} mode) with operating frequency of 2.45 GHz have not been investigated before. Therefore, this research studies the influence of vacuum pressure and operating microwave frequency to affect internal phenomena of unsaturated porous medium when apply microwave energy.

The objective of this study is carried out to predict temperature, microwave power absorbed and pressure buildup distribution, moisture profile, and movement of fluid inside the unsaturated porous media at vacuum and atmospheric pressures. Furthermore, the influence of material properties is investigated.

2. Experimental apparatus

Fig. 2 shows the experimental apparatus is used. The microwave system is a monochromatic wave of TE_{10} mode at operating frequency of 2.45 GHz. Microwave energy is generated by magnetron, and it is transmitted along z-direction of the rectangular waveguide with inside dimensions of 110 mm × 54.61 mm toward water load that is situated at the end of the waveguide. In addition,

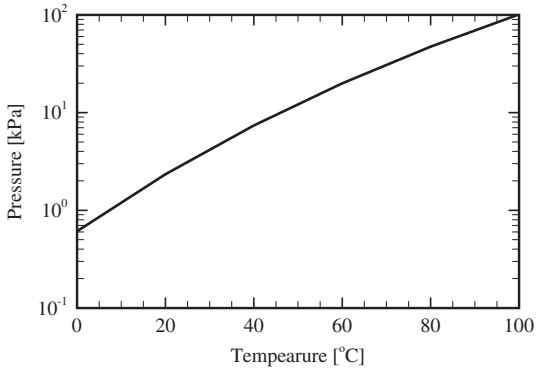

Fig. 1. Saturation vapor pressure of water as a function of temperature.

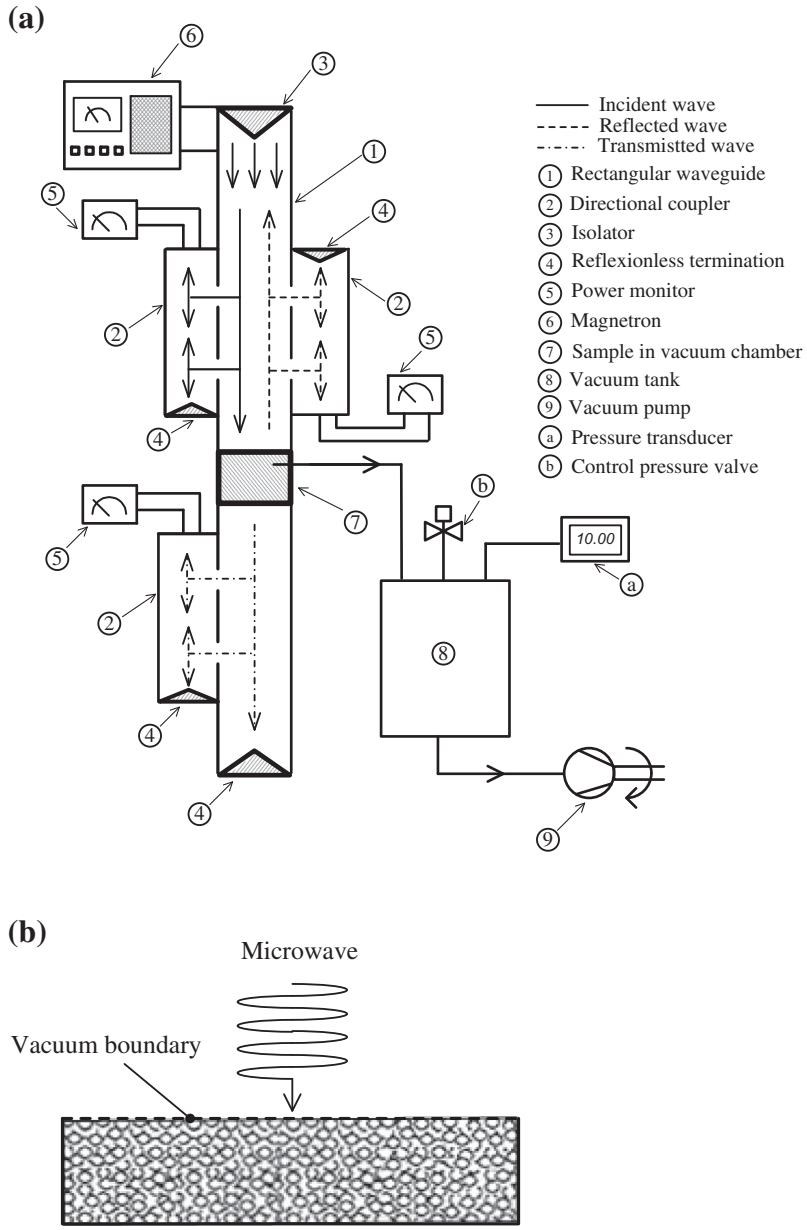

Fig. 2. Schematic of experimental apparatus: (a) a combined microwave and vacuum system, and (b) single-layered porous packed bed (sample) in rectangular waveguide.

an isolator is used to trap any microwave reflected from the sample to prevent it from damaging the magnetron. The powers of incident, reflected and transmitted waves were measured by a wattmeter using a directional coupler.

As shown in Fig. 2(c), the sample is a single-layered porous packed bed, which is composed of glass beads and water. A sample container is made from quartz. The sample of packed bed is inserted in the rectangular waveguide. The distributions of temperature within the sample are measured using fiber-optical temperature. The water saturations in the packed bed were defined as the fraction of the volume occupied by water to volume of the pores, and can be described in the following:

$$s = \frac{\rho_p(1-\phi)(m_w - m_d)}{\rho_l \phi m_d} \quad (1)$$

where s is water saturation, m_w and m_d are wet and dry mass of the sample, respectively, ϕ is porosity, ρ_l and ρ_p are densities of water and particle, respectively.

3. Analysis of mathematical modeling

Generally, studies on the microwave drying involve solutions of the equations governing electromagnetic propagation, i.e., Maxwell's equations, either by themselves or coupled with the heat transport equation. The surface of a sample is exposed to the monochromatic wave of TE_{10} mode with operating frequency of 2.45 GHz (shown as Fig. 2(a)).

3.1. Analysis of electromagnetic model

Fig. 3 shows the physical model used for analyzing microwave drying of capillary porous materials in a rectangular waveguide. The proposed model is based on the following assumptions:

(1) Since the microwave field in the TE_{10} mode has no variation of field in the direction between the broad faces, a two-dimensional model over the x–z plane is applicable to analysis of electromagnetic field inside a rectangular waveguide [22,23]

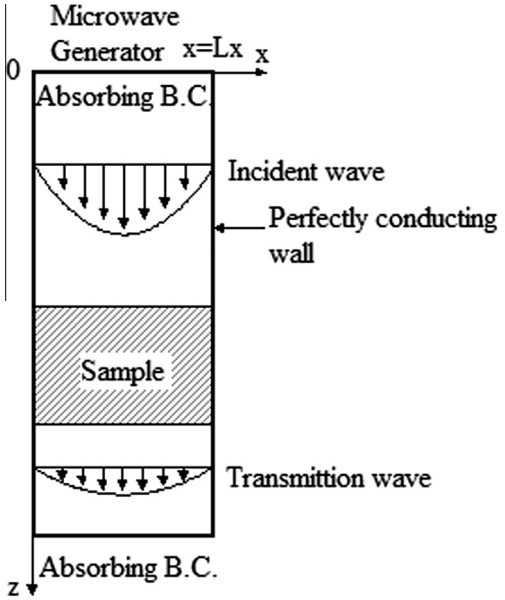

Fig. 3. Physical model for the microwave and dielectric material interactions inside a rectangular waveguide.

(2) The absorption of microwave energy by the cavity (including air) in the rectangular waveguide is negligible
(3) The walls of a rectangular waveguide are perfect conductors
(4) The effect of the sample container (made of quartz) on the electromagnetic field can be neglected because it did not absorb microwave energy

3.1.1. Basic equations of electromagnetic

The electromagnetic field is solved according to the theory of Maxwell's equations. In this study, the microwave of a fundamental TE_{10} mode is considered; therefore the Maxwell's equations in terms of the electric field intensity E and magnetic intensity H are given by:

$$\frac{\partial E_y}{\partial z} = \mu \frac{\partial H_x}{\partial t} \tag{2}$$

$$\frac{\partial E_y}{\partial x} = -\mu \frac{\partial H_z}{\partial t} \tag{3}$$

$$-\left(\frac{\partial H_z}{\partial_x} - \frac{\partial H_x}{\partial z}\right) = \sigma E_y + \varepsilon \frac{\partial E_y}{\partial t} \tag{4}$$

where the permittivity ε, magnetic permeability μ and electric conductivity σ as:

$$\varepsilon = \varepsilon_0 = \varepsilon_r, \quad \mu = \mu_0 \mu_r, \quad \sigma = 2\pi f \varepsilon \tan\delta \tag{5}$$

Additionally if magnetic effects are negligible, which is proven to be a valid assumption for most dielectric materials used in microwave heating applications, the magnetic permeability μ is well approximated by its value μ_0 in the free space. Let tan δ is the loss tangent

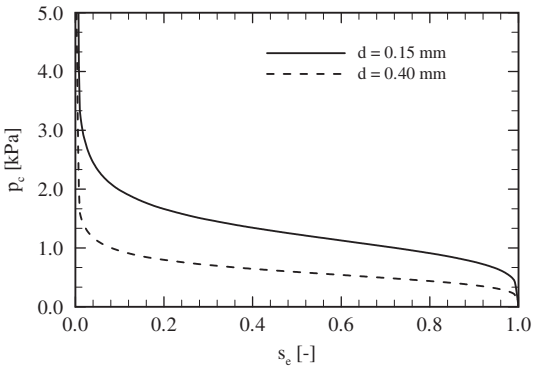

Fig. 5. Typical relationship between p_c and S_e.

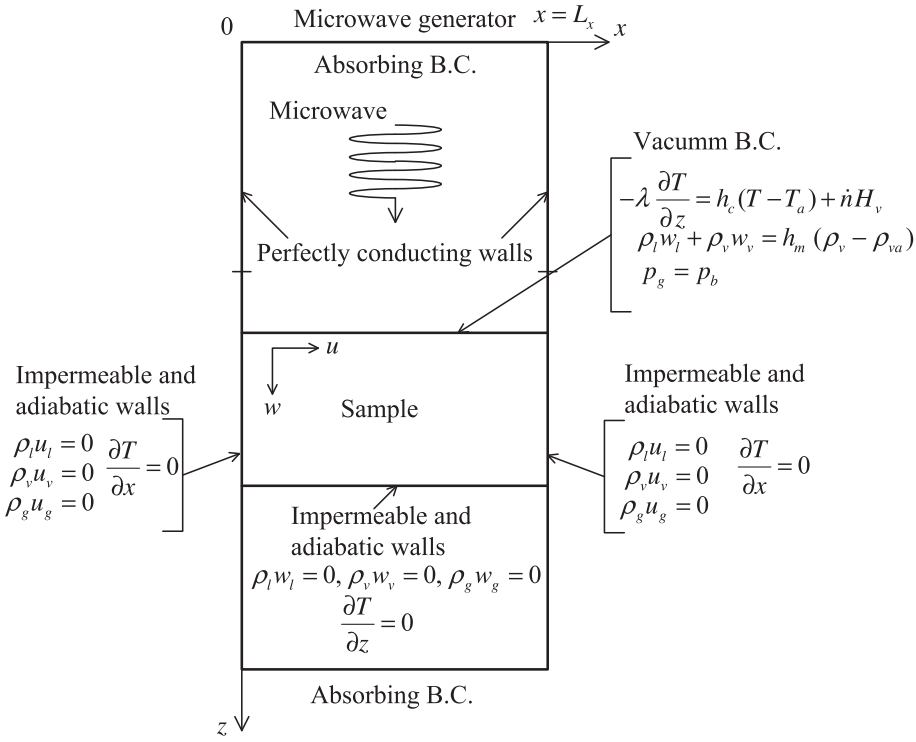

Fig. 4. Physical single layer model.

Table 1
Thermophysical and electromagnetic properties (at microwave frequency of 2.45 GHz) used in the computations.

Properties	Air	Water	Glass bead
ρ(kg/m^3)	1.205	1000.0	2500.0
C_p(J/kg K)	1.007	4.186	0.80
λ(W/m K)	0.0262	0.609	0.14
ε'_r(F/m)	1.0	$88.15 - 0.414T + 3.13\times10^{-3}T^2 - 4.60\times10^{-6}T^3$	5.1
$\tan\delta$ (–)	0.0	$0.323 - 9.499\times10^{-3}T + 1.27\times10^{-4}T^2 - 6.13\times10^{-2}T^3$	0.01

coefficient. In this work, the dielectric properties are assumed to vary with temperature only.

In this study, the effects on the overall drying kinetics are examined by selecting the dielectric properties as a function of moisture content and temperature. In order to determine the functional dependence of the combination of moisture content and temperature, the theory surrounding mixing formulas is used [24] in which the volume fractions (v) of water saturation, water vapor and glass particle were considered, as follows:

$$\varepsilon(s,T) = \varepsilon'(s,T) - j\varepsilon''(s,T) \tag{6}$$

where

$$[\varepsilon'(s,T)]^m = \sum_{i=1}^{3} v_i[\varepsilon'_{ri}(T)]^m = \phi.s[\varepsilon'_{rl}(T)]^m + = \phi(1-s)[\varepsilon'_{ra}]^m + (1-\phi)[\varepsilon'_{rp}]^m \tag{7}$$

$$[\varepsilon''(s,T)]^m = \sum_{i=1}^{3} v_i[\varepsilon''_i(T)]^m = \phi.s[\varepsilon''_{rl}(T)]^m + = \phi(1-s)[\varepsilon''_{ra}]^m + (1-\phi)[\varepsilon''_{rp}]^m \tag{8}$$

In above equations, the parameter m is likely to vary over the range 0–1, as suggested by Wang and Schmugge [24]. A value of $m = 0.33$ has been used throughout in this study. The loss tangent coefficient can be expressed as follow:

$$\tan\delta = \frac{\varepsilon''_r(s,t)}{\varepsilon'_r(s,t)} \tag{9}$$

When the material is heated unilaterally, it is found that as the dielectric constant and loss tangent coefficient vary, the penetration depth and the electric field within the dielectric material varies. The penetration depth is used to denote the depth at which the power

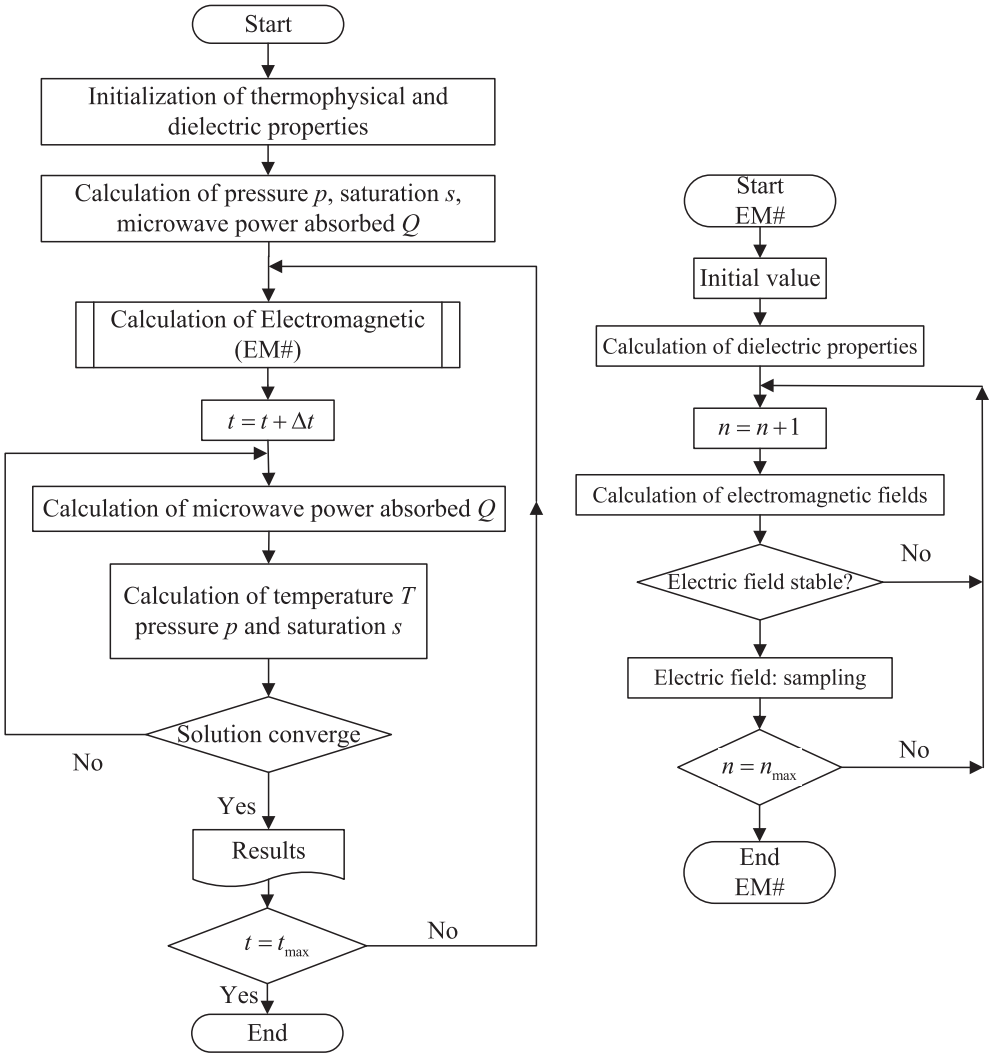

Fig. 6. Computational scheme.

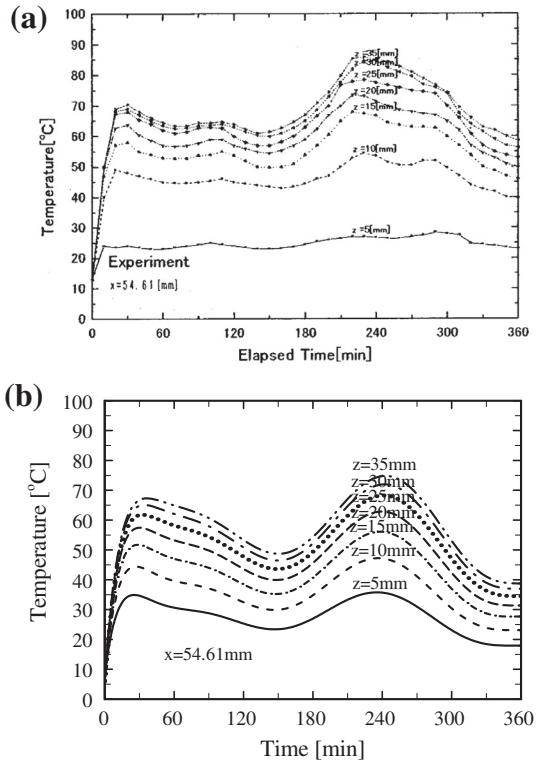

Fig. 7. Temperature profile in times at various depths ($P = 50$ W, $d = 0.15$ mm, $S_0 = 0.6$): (a) experiment result obtained by Ratanadecho et al. [26]; and (b) numerical result of the present study.

density has decreased to 37% of its initial value at the surface [25,26]

$$D_p = \frac{1}{\frac{2\pi f}{\upsilon}\sqrt{\frac{\varepsilon'_r\left(\sqrt{1+tan^2\delta}-1\right)}{2}}} \tag{10}$$

3.1.2. Boundary conditions

Corresponding to the physical model shown in Fig. 4, boundary conditions are given in the following list.

(a) Perfectly conducting boundaries; boundary conditions on the inner wall surface of a rectangular waveguide are given by using Faraday's law and Gauss' theorem:

$$E_t = 0, \quad H_n = 0 \tag{11}$$

where subscripts t and n denote the components of tangential and normal direction, respectively.

(b) Continuity boundary condition; boundary conditions along the interface between different materials, for example between air and dielectric material surface, are given by using Ampere's law and Gauss' theorem:

$$E_t = E'_t, \quad H_t = H'_t, \quad D_n = D'_n, \quad B_n = B'_n \tag{12}$$

where D is the electric flux density and B is the magnetic induction. The superscript $'$ denotes one of the different materials.

(c) Absorbing boundary condition; at both ends of the rectangular waveguide, the first order absorbing conditions proposed by Mur [27] are applied:

$$\frac{\partial E_y}{\partial t} = \pm\upsilon\frac{\partial E_y}{\partial z} \tag{13}$$

Here, the symbol ± represents forward or backward waves and υ is phase velocity of the microwave.

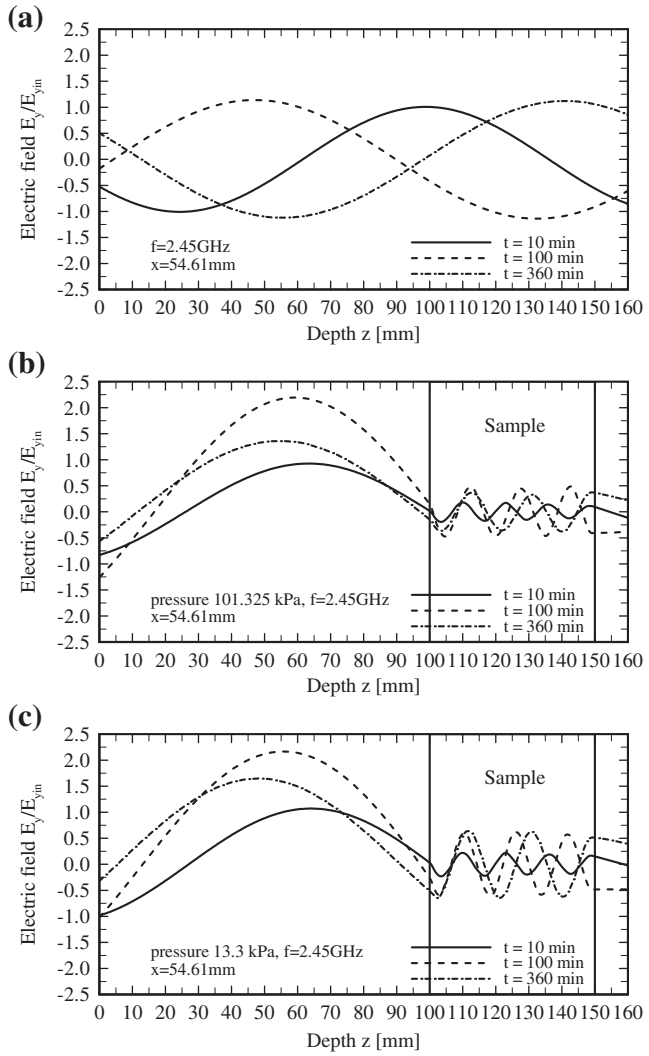

Fig. 8. Electric field distribution in case of microwave frequency of 2.45 GHz: (a) the rectangular waveguide is empty, (b) the sample is inserted in the waveguide rectangular at pressure of 101.325 kPa, (c) the sample is inserted in the rectangular waveguide at pressure of 13.3 kPa.

(d) Oscillation of the electric and magnetic field intensities by magnetron; incident wave due to magnetron is given by the following equations:

$$E_y = E_{yin}\sin\left(\frac{\pi x}{L_x}\right)\sin(2\pi ft) \tag{14a}$$

$$H_x = \frac{E_{yin}}{Z_H}\sin\left(\frac{\pi x}{L_x}\right)\sin(2\pi ft) \tag{14b}$$

where Z_H is the wave impedance defined as

$$Z_H = \frac{\lambda_g Z_I}{\lambda_0} = \frac{\lambda_g}{\lambda_0}\sqrt{\frac{\mu_0}{\varepsilon_0}} \tag{15}$$

3.2. Analysis of heat and mass transfer

A schematic diagram of model is illustrated in Fig. 4. By conservations of mass and energy in the capillary porous sample, the governing equation of mass and energy for all phases can be derived by using the volume average technique [28]. The main transport mechanisms that enable moisture movement during microwave

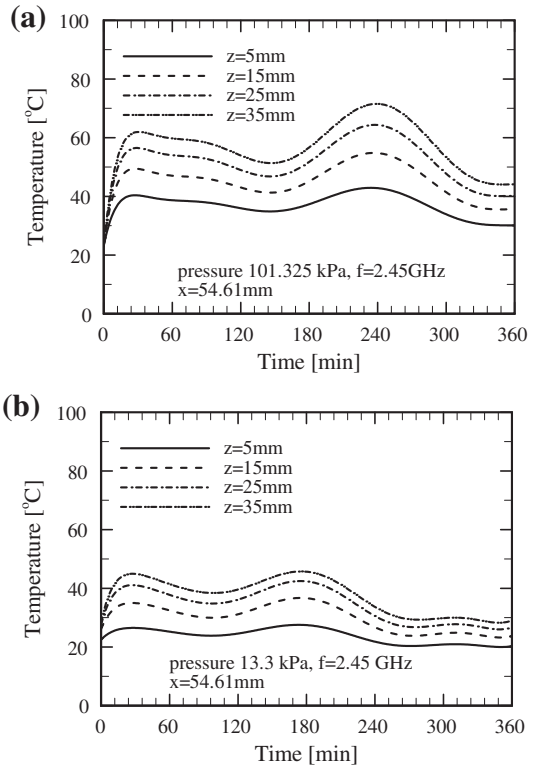

Fig. 9. Temperature profile in times with different z-depths at x-width of 54.61 mm: (a) atmospheric pressure, (b) vacuum pressure of 13.3 kPa.

drying of sample are: liquid flow driven by capillary pressure gradient and gravity while the vapor is driven by the gradient of the partial pressure of the evaporating species. The surface of the sample is exposed to external vacuum condition. Microwaves in the form of plane wave also incident on this surface. Other surfaces are insulated, and the heat and mass fluxes are set equal to zero. In this study, several simplifying assumptions are made in order to obtain a closed set of governing macroscopic equations:

(1) The capillary porous material is rigid, no chemical reactions take place in the sample.
(2) Local thermodynamic equilibrium is assumed.
(3) Simultaneous heat and mass transport occurs at a constant pressure, where the dominant mechanisms are capillary transport, vapor diffusion and gravity: such is generally the case in drying of capillary porous medium at specified vacuum pressure or atmospheric pressure when the temperature is lower than the boiling point.
(4) The gas binary mixture of air and water vapor behaves like an ideal gas.
(5) Darcy's law holds for the liquid and gas phases.
(6) Gravity is included for the liquid and gas phases.
(7) Permeability of liquid and gas can be expressed in term of relative permeability.
(8) The solid matrix is further assumed to be rigid and nondeformable.
(9) In a macroscopic sense, the porous packed bed is assumed to be homogeneous and isotropic, and water not bound to the solid matrix. Therefore, the volume average model for a homogeneous and isotropic material can be used in the theoretical modeling and analysis.
(10) Corresponding to electromagnetic field, temperature and moisture profiles also can be assumed to be two-dimensional in the x–z plane.

The governing equations based on a volume average approach led to the following conservation equations describing the drying process of capillary porous materials:

3.2.1. Mass conservation

The microscopic mass conservation equations for liquid, water vapor, and air phase, are written, respectively, as

$$\text{Liquid phase}: \quad \frac{\partial}{\partial t}(\rho_l \phi s) + \frac{\partial}{\partial x}(\rho_l u_l) + \frac{\partial}{\partial z}(\rho_l w_l) = -\dot{n} \tag{16}$$

$$\text{Vapor phase}: \quad \frac{\partial}{\partial t}[\rho_v \phi(1-s)] + \frac{\partial}{\partial x}(\rho_v u_v) + \frac{\partial}{\partial_z}(\rho_v w_v) = \dot{n} \tag{17}$$

$$\text{Air phase}: \quad \frac{\partial}{\partial t}[\rho_a \phi(1-s)] + \frac{\partial}{\partial x}(\rho_a u_a) + \frac{\partial}{\partial z}(\rho_a w_a) = 0 \tag{18}$$

where $\dot{n}$ is the condensation rate or evaporation rate during phase change and ϕ is the porosity of porous medium. The water vapor and air mass flux is the sum of the convective term with the gas superficial velocity and diffusive term. Additionally, the gas phase is assumed to be an ideal mixture of air and vapor phase.

3.2.2. Energy conservation

Ignoring kinetic energy and pressure terms which are usually unimportant, this can be obtained from the total energy conservation for a combined solid, water vapor and air phase and by invoking the assumption that local thermodynamic equilibrium prevails among the all phases, the temperature of the sample exposed to irradiation is obtained by solving the conventional heat transport equation with the microwave power absorbed included as a local electromagnetic heat generation term.

The governing energy equation describing the temperature rise in the sample is the time dependent equation:

$$\rho C_p \frac{\partial T}{\partial t} + \nabla[\{\rho C_{pl}\vec{u}_l + (\rho_a C_{pa} + \rho_v C_{pv})\vec{u}_g\}T] + H_v \dot{n} = -\nabla q + Q \tag{19}$$

where H_v is the latent heat of vaporization of water and Q is the microwave power absorbed term, which is a function of the electric field and defined as:

$$Q = 2\pi f \varepsilon_0 \varepsilon_r' (\tan\delta) E_y^2 \tag{20}$$

where ε_r' denotes relative dielectric constant, ε_0 denotes the permittivity of free space and tan δ denotes the loss tangent coefficient.

3.2.3. Phenomenological relation

In order to complete the system of equations, the expressions for the superficial average velocity of the liquid and gas phases the generalized Darcy's law in the following vector form is used:

$$\vec{u}_l = -\frac{KK_{rl}}{\mu_l}[\nabla p_g - \nabla p_c - \rho_l \vec{g}] \tag{21}$$

$$\vec{u}_g = -\frac{KK_{rg}}{\mu_g}[\nabla p_g - \rho_g \vec{g}] \tag{22}$$

The velocity of vapor water and air phase the generalized Fick's law for a two component gas mixture can be expressed in vector form as:

$$\rho_v \vec{u}_v = \rho_v \vec{u}_g - \rho_g D_m \nabla\left(\frac{\rho_v}{\rho_g}\right) \tag{23}$$

$$\rho_a \vec{u}_a = \rho_a \vec{u}_g - \rho_g D_m \nabla\left(\frac{\rho_v}{\rho_g}\right) \tag{24}$$

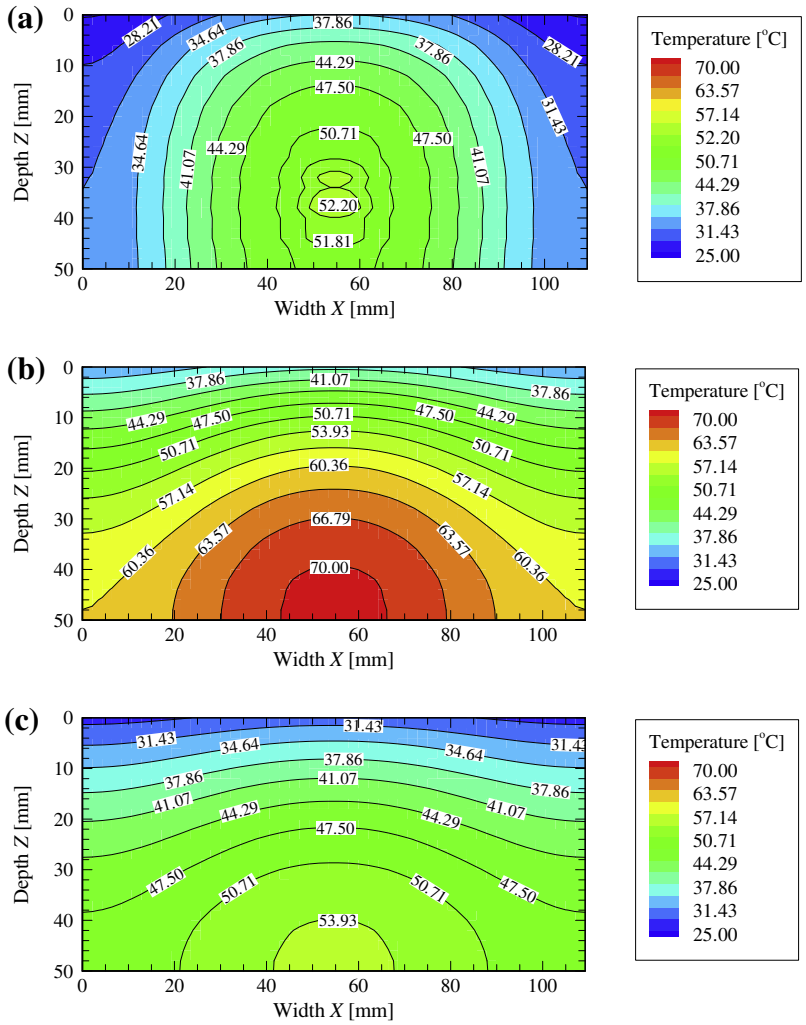

Fig. 10. Temperature distribution inside the sample at atmospheric pressure and microwave frequency of 2.45 GHz: (a) t = 10 min, (b) t = 100 min, and (c) t = 360 min.

where the capillary pressure p_c is related to the gas and liquid phases can be written by

$$p_c = p_g - p_l \tag{25}$$

and D_m is the effective molecular mass diffusion [29] as:

$$D_m = \frac{2\phi}{3-\phi}(1-s)D \tag{26}$$

where D is the binary mass diffusion in plain media, and can be defined as:

$$D = D_0\left(\frac{p_0}{p}\right)\left(\frac{T}{T_0}\right)^{2.2} \tag{27}$$

Fourier's law is used to define the heat flux through the porous material

$$q = -\lambda_{eff}\nabla T \tag{28}$$

3.2.4. Equilibrium relation

The system of conservation equations obtained for multiphase transport mode requires constitutive equation for relative permeability K_r, capillary pressure p_c, capillary pressure functions or Leverett functions $J(s_e)$, and the effective thermal conductivity λ_{eff}. A typical set of constitutive relationships for liquid and gas system is given by Kaviany and Mittal [30]

$$K_{rl} = s_e^3, K_{rg} = (1-s_e)^3 \tag{29}$$

where s_e is the effective water saturation considered the irreducible water saturation s_{ir} and defined by

$$s_e = \frac{s - s_{ir}}{1 - s_{ir}} \tag{30}$$

The capillary pressure p_c is further assumed to be a function of water saturation or Leverett functions $J(s_e)$ and surface tension $\xi(T)$. The Leverett functions $J(s_e)$ is dependent on the internal structure of the porous materials and defined by Aoki et al. [31]:

$$J(s_e) = 0.325(1/s_e - 1)^{0.217} \tag{31}$$

The relationship between the capillary pressure and the water saturation is defined by using Leverett functions $J(s_e)$:

$$p_c = p_g - p_l = \frac{\xi}{\sqrt{K/\phi}}J(s_e) \tag{32}$$

where K the permeability of capillary porous materials is found from the Carman–Kozeny equation [32]:

$$K = \frac{d^2}{180}\frac{\phi^3}{(1-\phi)^2} \tag{33}$$

Fig. 5 shows the typical moisture characteristic curve for different particle sizes obtained from present experiments. It is seen that,

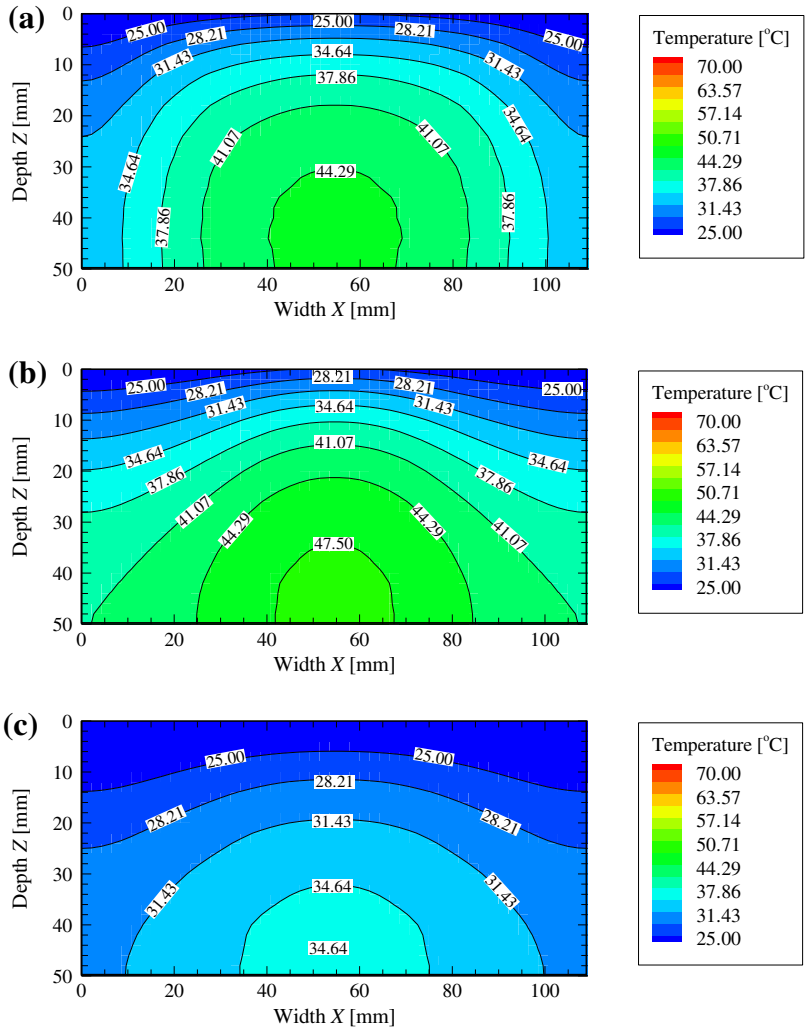

Fig. 11. Temperature distribution inside the sample at vacuum pressure of 13.3 kPa and microwave frequency of 2.45 GHz: (a) t = 10 min, (b) t = 100 min, and (c) t = 360 min.

in the case of the same water saturation, a smaller particle size corresponds to a higher capillary pressure.

Based on the experimental results of Aoki et al. [31] using a glass beads unsaturated with water, the effective thermal conductivity is further assumed to be a function of water saturation and defined by

$$\lambda_{eff} = \frac{0.8}{1 + 3.78e^{-5.95s}} \tag{34}$$

3.2.5. State equation

The gas phase is assumed to be an ideal mixture of perfect gases, so that the species density can be determined by the state equations, with the classical definitions for total density of the gas, ρ_g, and the mass average velocity of the gas:

$$\rho_a = \frac{p_a M_a}{R_0 T} \tag{35}$$

$$\rho_v = \frac{p_v M_v}{R_0 T} \tag{36}$$

$$\rho_g = \rho_a + \rho_v \tag{37}$$

$$p_a = \rho_a R_a T \tag{38}$$

$$P_v = \rho_v R_v T \tag{39}$$

$$p_g = p_a + p_v \tag{40}$$

$$\rho_g u_g = \rho_a u_a + \rho_v u_v \tag{41}$$

The partial pressure of the vapor is given by Kelvin's equation considered the capillary force defined by:

$$p_v = p_{vs} exp\left(\frac{p_c}{\rho_l R_v T}\right) \tag{42}$$

where p_{vs} is the partial pressure of the saturation vapor as a function of temperature [14,33] that shown in Fig. 1 and defined by

$$p_{vs} = C_0 + C_1 T + C_2 T^2 + C_3 T^3 + C_4 T^4 + C_5 T^5 \tag{43}$$

where

$$C_0 = 610.8, \quad C_1 = 43.87, \quad C_2 = 1.47, \quad C_3 = 0.025,$$
$$C_4 = 2.88 \times 10^{-4}, \quad C_5 = 2.71 \times 10^{-6}$$

3.2.6. Moisture transport equation

The phenomenon of moisture transport in the sample is described by the mass conservation equations for the liquid phase (Eq. (15)), and the vapor portion of the gas phase (Eq. (16)). Since the total water content is interested, these equations in two-dimensional scalar forms can be added together to yield an equation for the total moisture content as follows:

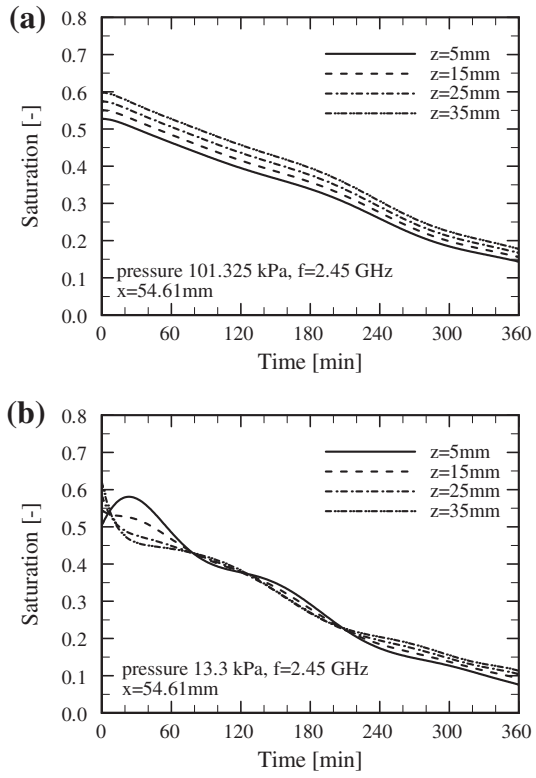

Fig. 12. Saturation profile in times with different z-depths at x-width of 54.61 mm: (a) atmospheric pressure, (b) vacuum pressure of 13.3 kPa.

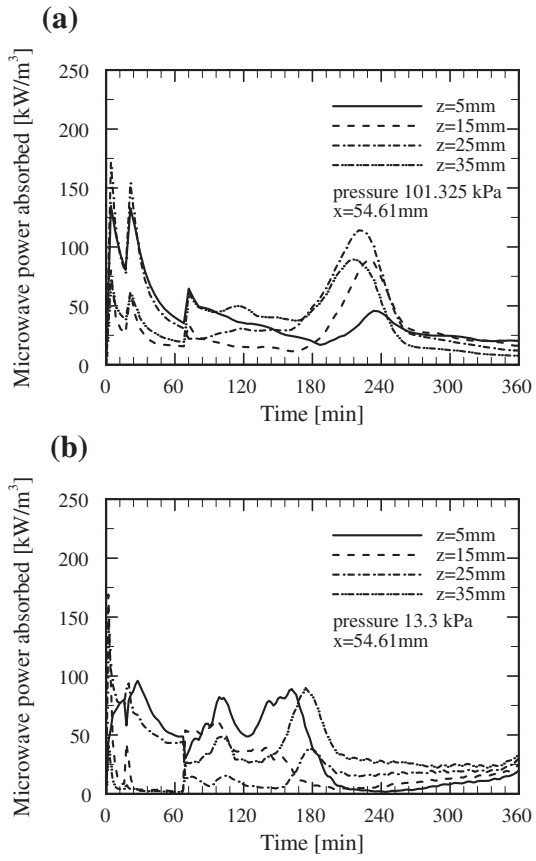

Fig. 13. Microwave power absorbed profile in times with different z-depths at x-width of 54.61 mm: (a) atmospheric pressure, (b) vacuum pressure of 13.3 kPa.

$$\phi\frac{\partial}{\partial t}[\rho_l s+\rho_v(1-s)]+\frac{\partial}{\partial x}(\rho_l u_l+\rho_v u_v)+\frac{\partial}{\partial z}(\rho_l w_l+\rho_v w_v)=0 \tag{44}$$

Using Darcy's generalized equation (Eqs.(20) and (21)) and Fick's law (Eqs.(22) and (23)), the moisture transport equation is written as:

$$\begin{aligned}&\phi\frac{\partial}{\partial t}[\rho_l s+\rho_v(1-s)]\\&+\frac{\partial}{\partial x}\left[\rho_l\frac{KK_{rl}}{\mu_l}\left(\frac{\partial p_c}{\partial x}-\frac{\partial p_g}{\partial x}+\rho_l g_x\right)+\rho_v\frac{KK_{rg}}{\mu_g}\left(-\frac{\partial p_g}{\partial x}+\rho_g g_x\right)-D_m\frac{\partial \rho_v}{\partial x}\right]\\&+\frac{\partial}{\partial z}=\left[\rho_l\frac{KK_{rl}}{\mu_l}\left(\frac{\partial p_c}{\partial_z}-\frac{\partial p_g}{\partial_z}+\rho_l g_z\right)+\rho_v\frac{KK_{rg}}{\mu_g}\left(-\frac{\partial p_g}{\partial z}+\rho_g g_z\right)-D_m\frac{\partial \rho_v}{\partial z}\right]=0\end{aligned} \tag{45}$$

In addition, it is assumed that gravitational effect in x-direction is negligible. Thus, Eq. (38) becomes:

$$\begin{aligned}&\phi\frac{\partial}{\partial t}\{\rho_l s+\rho_v(1-s)\}\\&+\frac{\partial}{\partial x}\left[\rho_l\frac{KK_{rl}}{\mu_l}\left(\frac{\partial p_c}{\partial x}-\frac{\partial p_g}{\partial x}\right)+\rho_v\frac{KK_{rg}}{\mu_g}\left(-\frac{\partial p_g}{\partial x}\right)-D_m\frac{\partial \rho_v}{\partial x}\right]\\&+\frac{\partial}{\partial z}\left[\rho_l\frac{KK_{rl}}{\mu_l}\left(\frac{\partial p_c}{\partial z}-\frac{\partial p_g}{\partial x}+\rho_l g_z\right)+\rho_v\frac{KK_{rg}}{\mu_g}\left(-\frac{\partial p_g}{\partial x}+\rho_g g_z\right)-D_m\frac{\partial \rho_v}{\partial z}\right]=0\end{aligned} \tag{46}$$

3.2.7. Total pressure equation

Considering the Darcy's law and Fick's law, and assuming that the gaseous phase is an ideal mixture of perfect gases, Eq. (17) becomes:

$$\begin{aligned}&\phi\frac{\partial}{\partial t}[\rho_a(1-s)]+\frac{\partial}{\partial x}\left[\rho_a\frac{KK_{rg}}{\mu_g}\left(-\frac{\partial p_g}{\partial x}\right)-D_m\frac{\partial}{\partial x}(\rho_a)\right]\\&+\frac{\partial}{\partial z}\left[\rho_a\frac{KK_{rg}}{\mu_g}\left(-\frac{\partial p_g}{\partial z}+\rho_g g_z\right)-D_m\frac{\partial}{\partial z}(\rho_a)\right]=0\end{aligned} \tag{47}$$

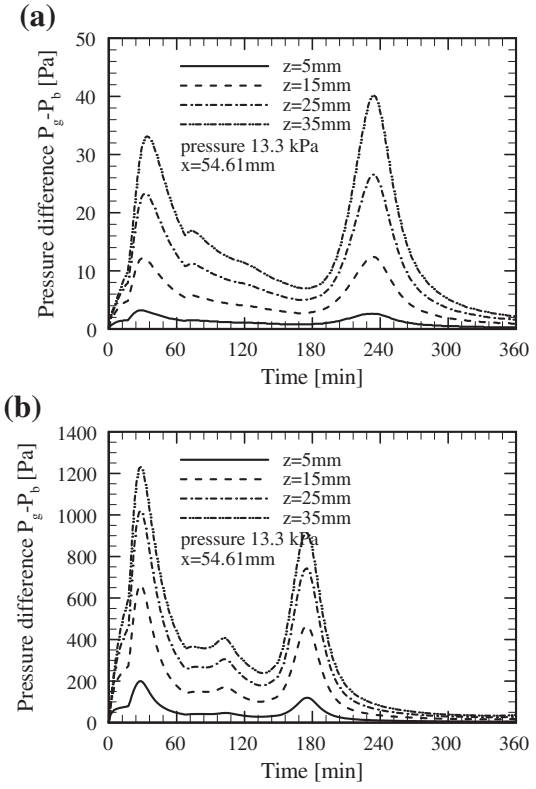

Fig. 14. Pressure difference profile in times with different z-depths at x-width of 54.61 mm: (a) atmospheric pressure, (b) vacuum pressure of 13.3 kPa.

3.2.8. Heat transport equation

For a nonisothermal flow, we must add temperature as a dependent variable. The conservation of energy equation for the two-dimensional model allows prediction of the temperature. Thus, Eq. (18) leads to:

$$\rho C_p \frac{\partial T}{\partial t} + \frac{\partial}{\partial x}\left[\{\rho_l C_{pl} u_l + (\rho_a C_{pa} + \rho_v C_{pv}) u_g\} T\right] + \frac{\partial}{\partial z}\left[\{\rho_l C_{pl} w_l + (\rho_a C_{pa} + \rho_v C_{pv}) w_g\} T\right] + H_v \dot{n} = \frac{\partial}{\partial x}\left[\lambda_{eff} \frac{\partial T}{\partial x}\right] + \frac{\partial}{\partial z}\left[\lambda_{eff} \frac{\partial T}{\partial z}\right] + Q \quad (48)$$

where ρC_p is the effective heat capacitance of water–gas matrix mixtures:

$$\rho C_p = \rho_l C_{pl} \phi s + (\rho_a C_{pa} + \rho_v C_{pv}) \phi (1 - s) + \rho_p C_{pp} (1 - \phi) \quad (49)$$

Also, the phase change term is given by

$$\dot{n} \frac{\partial}{\partial t}\{\rho_v \phi (1 - s)\} + \frac{\partial}{\partial x}\left[-D_m \frac{\partial \rho_v}{\partial x}\right] + \frac{\partial}{\partial z}\left[\rho_v \frac{KK_{rg}}{\mu_g} \rho_g g_z - D_m \frac{\partial \rho_v}{\partial z}\right] \quad (50)$$

3.2.9. Boundary and initial conditions

In Fig. 4 two types of boundary conditions for solution of the governing equations are formulated at the open and impermeable boundaries. At open boundary (as vacuum boundary), the liquid and vapor flux reaching the boundary from the interior is fully evaporated and convected away as vapor to the ambient. Regardless of the volumetric evaporation rate inside, any remaining liquid flux arriving at the surface is evaporated at the open boundary. The exchanger of energy at the open boundary which can be described in the following form:

$$-\lambda_{eff} \frac{\partial T}{\partial z} = h_c (T - T_\infty) + \dot{n} H_v \quad (51)$$

where h_c is the local heat transfer coefficient, and T_∞ is the reference temperature in the gas phase surrounding the vacuum boundary.

Mass transfer at the open boundary is modeled by means of a locally constant mass transfer coefficient, which is related to the local vapor flux density, and is described as:

$$\rho_l w_l + \rho_v w_v = h_m (\rho_v - \rho_\infty) \quad (52)$$

where ρ_v is the density of vapor at the open boundary and ρ_∞ is reference vapor density in the gas phase surrounding the open bound-

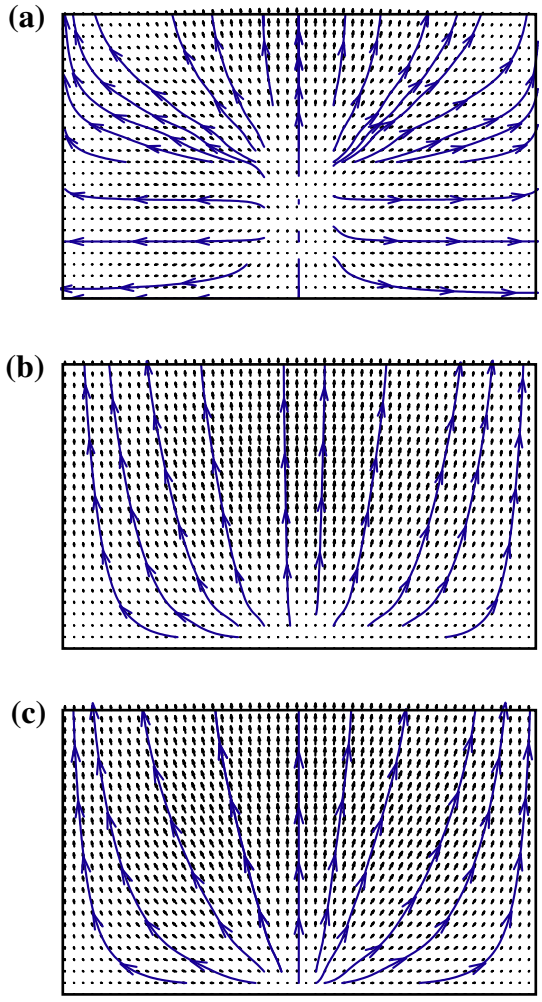

Fig. 15. Vector and streamline of vapor flux inside the sample at atmospheric pressure (scale × 9,000,000): (a) t = 10 min, (b) t = 100 min, and (c) t = 360 min.

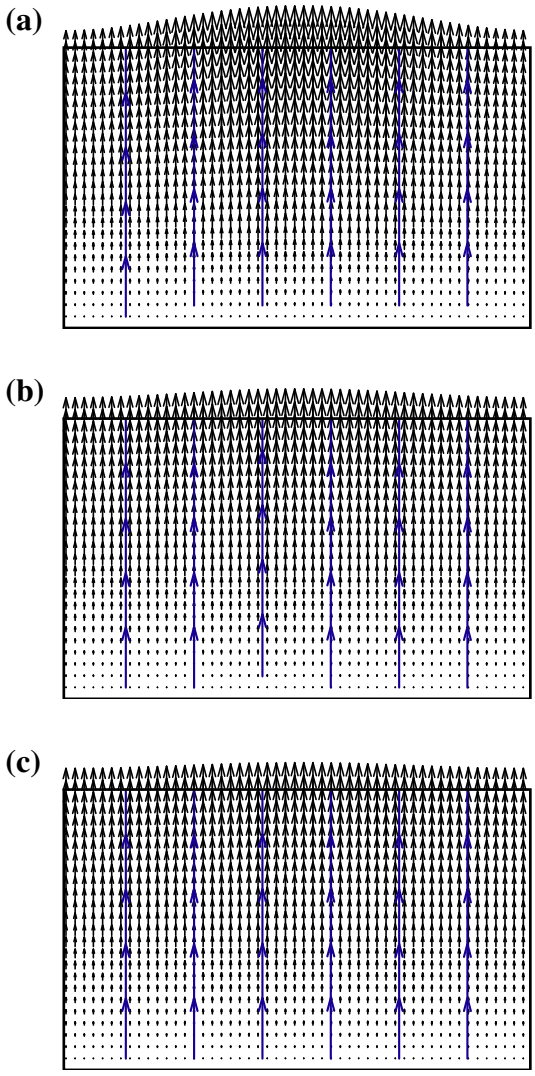

Fig. 16. Vector and streamline of liquid flux inside the sample at atmospheric pressure (scale × 2500): (a) t = 10 min, (b) t = 100 min, and (c) t = 360 min.

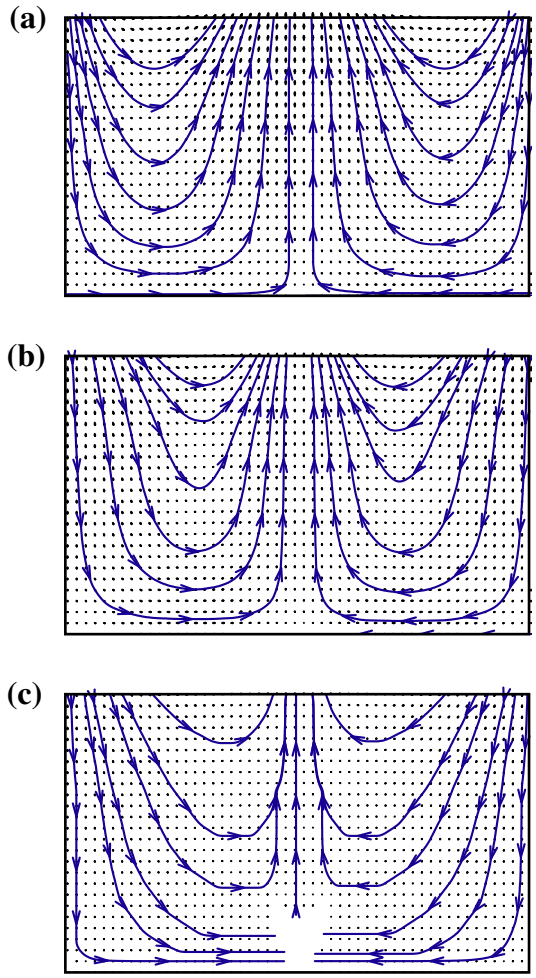

Fig. 17. Vector and streamline of air flux inside the sample at atmospheric pressure (scale × 30,000,000): (a) t = 10 min, (b) t = 100 min, and (c) t = 360 min.

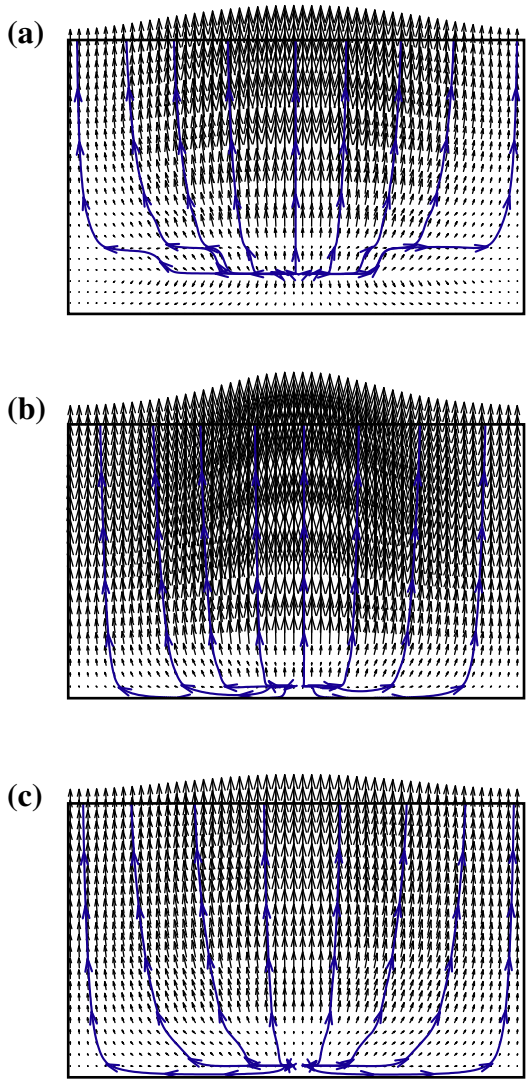

Fig. 18. Vector and streamline of vapor flux inside the sample at vacuum pressure of 13.3 kPa (scale × 9,000,000): (a) t = 10 min, (b) t = 100 min, and (c) t = 360 min.

ary, and assuming in this case the analogy between heat and mass transfer [32], the local mass transfer coefficient, h_m can be expressed as:

$$h_m = \frac{h_c}{\rho_g C_{pg} Le^{2/3}} \tag{53}$$

where

$$Le = \frac{\alpha_g}{D} \tag{54}$$

The total pressure at open boundary (the external drying surface) is fixed at boundary pressure, p_b as:

$$p_g = p_b \tag{55}$$

where p_b is equal to or less than 101.325 kPa in case of atmospheric pressure and vacuum pressure, respectively. Considering boundary conditions at the impermeable boundary that no heat and mass exchange taken place are given by:

$$\frac{\partial T}{\partial x} = \frac{\partial T}{\partial z} = 0, \quad \rho u = \rho w = 0 \tag{56}$$

The initial conditions are given by uniform initial temperature and moisture content.

4. Numerical solution procedure

4.1. Model discretization

The description of heat, mass transfer and total pressure equations (Eqs. (39)–(41)) requires specification of temperature (T), total pressure (p_g) and the moisture content (s) within the sample. These equations are coupled to the Maxwell equations (Eqs. (2)–(4) by Eq. (19)). The later equation represents the local microwave power absorbed in the sample.

In order to predict the electromagnetic field (Eqs. (2)–(4)), a finite difference time domain (FDTD) method is applied. The system of nonlinear partial differential equations (Eqs. (39)–(41)) are solved by a finite difference method. The Newton Raphson method is employed at each iteration to quicken the convergence. Initially, the temperature and moisture profiles were set to be equal at all nodes at values corresponding to the measured capillary porous medium conditions. Considering the microwave drying in TE_{10} mode, it is the lowest mode of the supported microwave field for waves transmitted in the present rectangular waveguide without power dissipation. The type of wave mode is prescribed by the frequency and waveguide dimension.

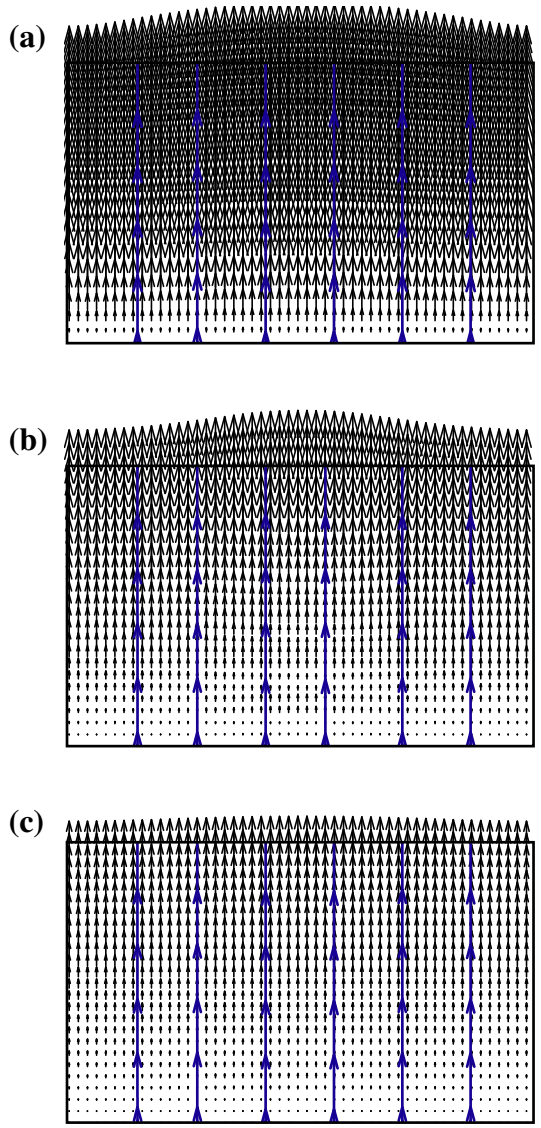

Fig. 19. Vector and streamline of liquid flux inside the sample at vacuum pressure of 13.3 kPa (scale × 2500): (a) t = 10 min, (b) t = 100 min, and (c) t = 360 min.

4.2. The stability and accuracy of calculation

Spatial and temporal resolution is selected to ensure of stability and accuracy. Eqs. (2)–(4) are solved on a grid system, and temporally they are solved alternatively for both the electric and magnetic fields. To insure stability of the time-stepping algorithm, Δt was chosen to satisfy the courant stability condition:

$$\Delta t \leq \frac{\sqrt{(\Delta x)^2 + (\Delta z)^2}}{\upsilon} \tag{57}$$

and the spatial resolution of each cell defined as

$$\Delta x, \Delta z \leq \frac{\lambda_g}{10\sqrt{\varepsilon_r}} = \frac{\lambda_{mg}}{10} \tag{58}$$

The relative errors in the iteration procedure of 10^{-8} are chosen. One aspect of model verification is to compare drying data from experiments run under different conditions with mathematical simulations using parameter values obtained from Table 1. The details of computational scheme and strategy are illustrated in Fig. 6.

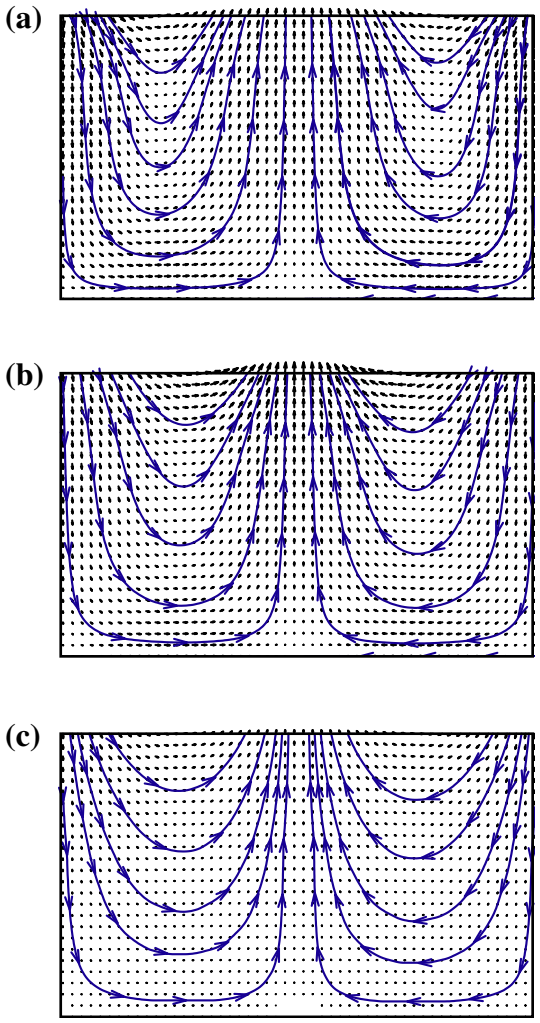

Fig. 20. Vector and streamline of air flux inside the sample at vacuum pressure of 13.3 kPa (30,000,000): (a) t = 10 min, (b) t = 100 min, and (c) t = 360 min.

5. Results and discussion

The numerical results for heat, multiphase flow and pressure buildup in an unsaturated porous packed bed (composed of glass beads, water, and air) filled in a rectangular waveguide and subjected to a combined microwave and vacuum system are investigated. A microwave system supplies a monochromatic wave in a fundamental mode (TE_{10} mode) with operating frequency of 2.45 GHz and input microwave power of 50 W.

5.1. Numerical validation

Fig. 7(a) and (b) shows the present simulation results compared with experimental data from Ratanadecho et al. [26] of temperature profiles within the sample, corresponding to the initial temperature of 10.4 °C, initial saturation s_{in} of 0.6, particle size d_p of 0.15 mm and input microwave power of 50 W. It is observed that the trends of results are in good agreement. The source of the discrepancy is the non-uniform heating effect along the axis, which accounts for the fact that the incident microwave at the surface of the sample is non-uniform. Numerically, the discrepancy may be attributed to uncertainties in the thermal and dielectric property database. On the other hand during the experiment of microwave drying process, the impact on the uncertainty of our data

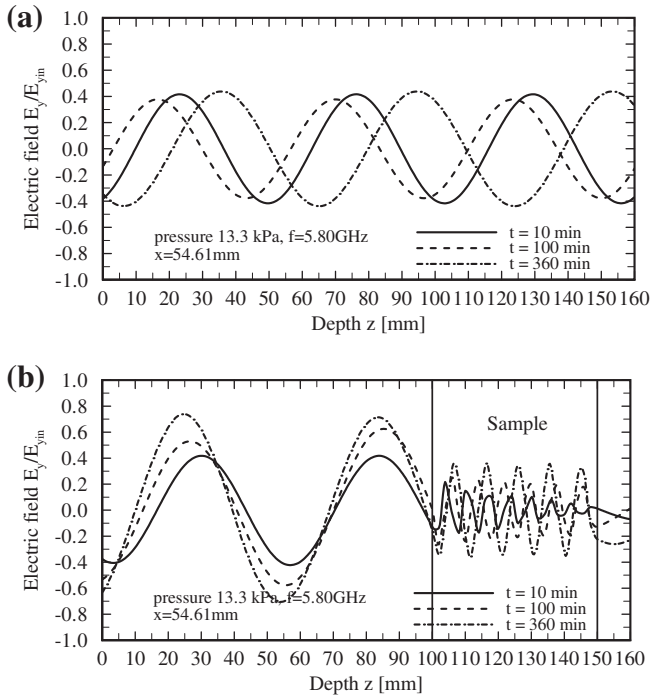

Fig. 21. Electric field distribution in case of vacuum pressure of 13.3 kPa and microwave frequency of 5.8 GHz: (a) the rectangular waveguide is empty, (b) the sample is inserted in the rectangular waveguide.

Table 2
Penetration depth of unsaturated packed bed at various times.

Time (min)	Penetration depth D_p (mm)	
	f = 2.45 GHz	f = 5.80 GHz
0	200.12	52.18
10	265.73	57.02
100	377.09	94.86
360	946.67	258.62

may cause by variations in humidity, room temperature and another effects.

5.2. The effect of vacuum pressure level

The numerical results for heat, multiphase flow and pressure buildup in an unsaturated porous packed bed subjected to microwave energy are investigated at vacuum pressure of 13.3 kPa (100 torr) compared with atmospheric pressure condition. However, two drying processes using the operating microwave frequency of 2.45 GHz, the input microwave power of 50 W, initial temperature of 25 °C, initial saturation of 0.6, and particle size of 0.15 mm are selected. In the selected vacuum pressure of 13.3 kPa is in typical range of pressure (1.33–26.66 kPa) in vacuum processing and is similar to Changrue [34] in which microwave vacuum processing is applied to investigate drying of carrots cubes. The input microwave power of 50 W is also lower than the critical breakdown electric field [2]. Therefore, the effect of gas breakdown is not appeared in this drying condition.

Fig. 8(a) illustrates the electric field distribution along the center axis (x = 54.61 mm) of the empty rectangular waveguide at different drying times (t = 10, 100 and 360 min) in case of atmospheric pressure which is similar to vacuum pressure of 13.3 kPa. In this figure, the vertical axis represents the intensity of the electric fields E_y, which is normalized to the amplitude of

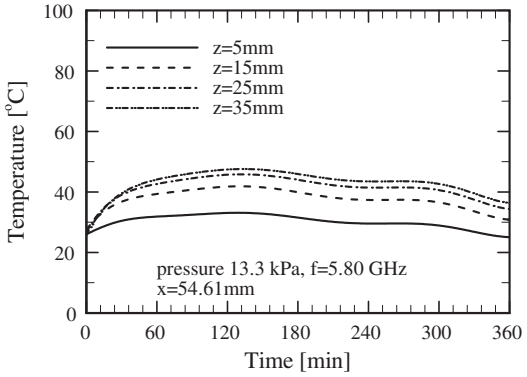

Fig. 22. Temperature profile in times with different z-depths at x-width of 54.61 mm in case of vacuum pressure of 13.3 kPa and microwave frequency of 5.80 GHz.

the input electric fields E_{yin}, it is seen that the stationary wave inside the empty waveguide with completely power is absorbed by water load at the end of the waveguide.

Fig. 8(b) and (c) shows the electric filed distribution along the center axis (x = 54.61 mm) of the rectangular waveguide when inserted the sample at different drying times (t = 10, 100 and 360 min) in case of atmospheric pressure and vacuum pressure of 13.3 kPa, respectively. Since the sample is composed of glass beads, water and air that is implied to be a lossy material (moist porous material). For the case of atmospheric pressure, it is observed from Fig. 8(b) that the resonance of standing wave configuration inside the sample is weak as compared to left-hand side of the sample. Focusing attention of the electric filed distribution inside the cavity (left-hand side), a stronger standing wave with large amplitude is formed by interference between the incident waves and reflected waves from the surface of sample due to the different dielectric properties of materials (air and sample) at the interface. It is evident from the results that the electric filed distribution within the sample attenuates owing to the microwave power absorbed, and thereafter the microwave power absorbed is converted to the thermal energy. The some part of microwaves is transmitted through the sample and then absorbed by water load at the end of the waveguide. At drying time t = 10 min, the sample having moist porous material, the electric field attenuates due to microwave power absorbed to the sample and then the microwave power absorbed is converted to thermal energy, causing increase temperature within the sample. Furthermore the electric field within the sample is almost extinguished lead to short wavelength and small amplitude of electric field. As drying proceed t = 100 and 360 min, a majority of the moist content has been removed, the effect of reflected waves from the surface of sample is reduced which increases the large part of microwaves inside the sample. Consequently, the reflected and transmitted wave at each interface will contribute to the resonance of standing wave configuration with the larger amplitude and wavelength inside the sample where the moisture content is small in comparison with early stage of drying time (t = 10 min).

For the case of vacuum pressure of 13.3 kPa (as seen in Fig. 8(c)), the electric fields with small amplitude are formed within the sample, while the stronger standing wave outside the sample (left-hand side) with a lager amplitude is formed by interference between the incident waves and reflected waves from the surface of sample. In addition, the electric field within the sample attenuates owing to microwave power absorbed, and thereafter the microwave power absorbed is converted to thermal energy (similar to atmospheric pressure condition). However, it is interesting to observe that the electric field intensity in case of vacuum

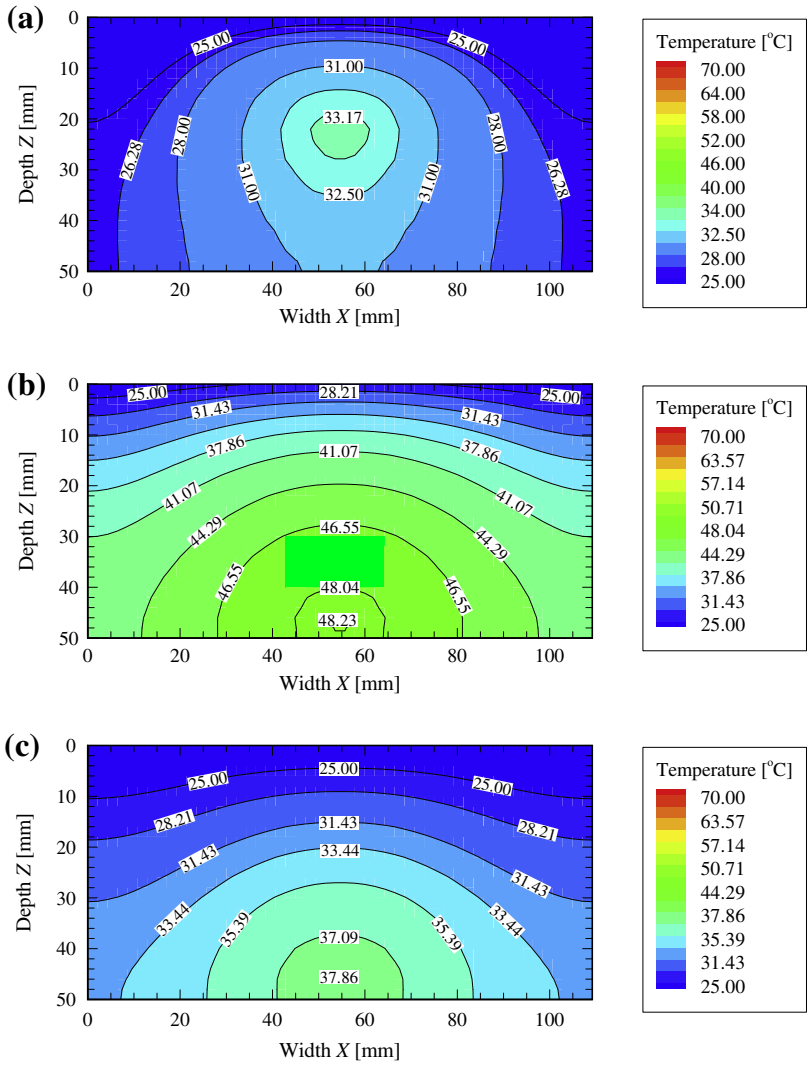

Fig. 23. Temperature distribution inside the sample at vacuum pressure of 13.3 kPa and microwave frequency of 5.80 GHz: (a) t = 10 min, (b) t = 100 min, and (c) t = 360 min.

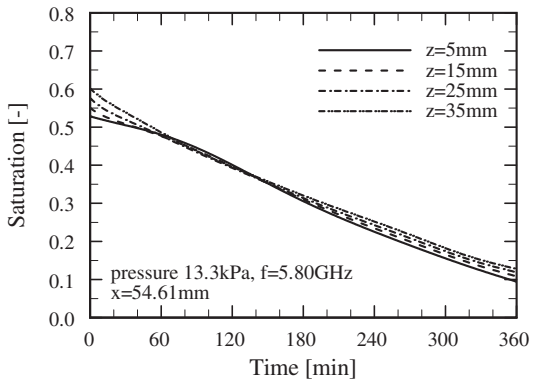

Fig. 24. Saturation profile in times with different z-depths at x-width of 54.61 mm in case of vacuum pressure of 13.3 kPa and microwave frequency of 5.80 GHz.

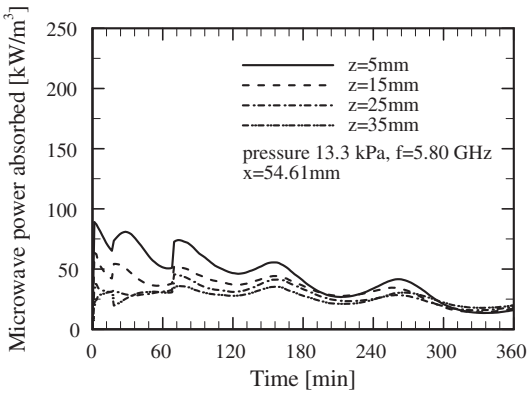

Fig. 25. Microwave power absorbed profile in times with different z-depths at x-width of 54.61 mm in case of vacuum pressure of 13.3 kPa and microwave frequency of 5.80 GHz.

pressure of 13.3 kPa is greater than in case of atmospheric pressure when drying proceed (such as t = 100 and 360 min). This is because moisture content is removed with higher rate as compared to atmospheric pressure.

Fig. 9 shows temperature profile at various times in case of vacuum pressure of 13.3 kPa and atmospheric pressure. In contrast to that in a conventional drying, a microwave drying provides higher temperature inside the drying sample while the surface temperature stays colder due to effect of surrounding air. At same time the evaporation takes place at the surface of sample at lower temperature due to evaporative cooling. It is seen that the temperature

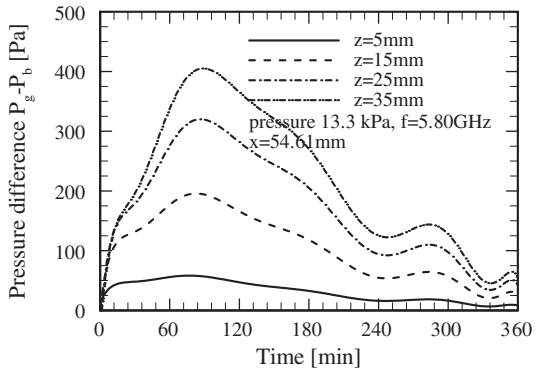

Fig. 26. Pressure difference profile in times with different z-depths at x-width of 54.61 mm in case of vacuum pressure of 13.3 kPa and microwave frequency of 5.80 GHz.

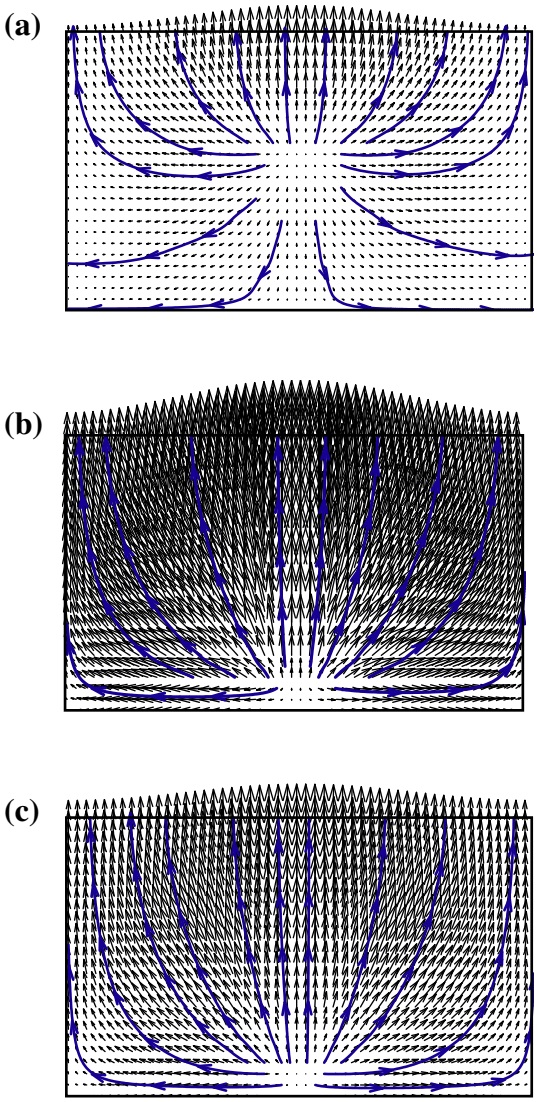

Fig. 27. Vector and streamline of vapor flux inside the sample at vacuum pressure of 13.3 kPa and microwave frequency of 5.80 GHz (scale × 9,000,000): (a) t = 10 min, (b) t = 100 min, and (c) t = 360 min.

profile within the sample rise up steadily in the early stages of drying. Due to the large initial moisture content, the skin depth heating effect causes a majority of microwave to be decay, resulting in a

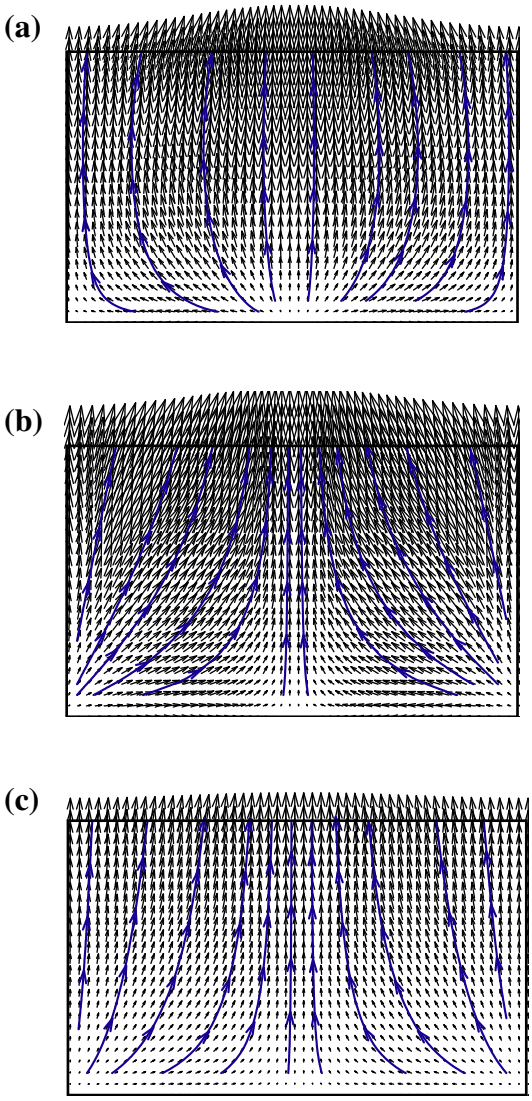

Fig. 28. Vector and streamline of liquid flux inside the sample at vacuum pressure of 13.3 kPa and microwave frequency of 5.80 GHz (scale × 2,500): (a) t = 10 min, (b) t = 100 min, and (c) t = 360 min.

lower rate of microwave power absorbed in the interior. As the drying process proceeds, moisture content is removed from the sample; the microwave can penetrate further into the sample as material dries. During this state of drying, temperature profile slows down considerably because moisture inside the sample is significant reduced, reducing dielectric loss factor as well as microwave power absorbed also. Nevertheless, temperature profiles at vacuum pressure are lower than atmospheric pressure as shown in Figs. 9–11 because the boiling point of water is fallen down under vacuum condition. It is found that at vacuum pressure of 13.3 kPa, water evaporation takes place within the sample and the temperature of sample is always lower than the boiling point of water which is equal to 56.02 °C. Consequently the sample processing temperature can be significant lower than atmospheric condition.

Fig. 12 presents the moisture profile in term of saturation profile at vacuum and atmospheric pressure. In the early state of drying, the internal movement of moisture is due to liquid flow by capillary action and vapor flow by molecular diffusion. As the drying process proceeds, the capillary action plays an important role in the moisture migration mechanism and maintains a good supply of liquid to the surface, and would cause the average moisture

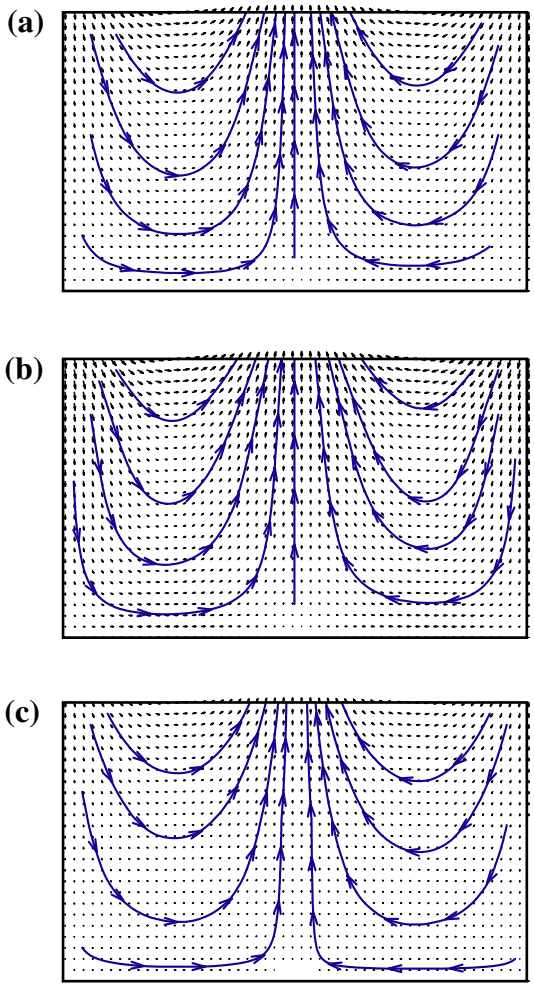

Fig. 29. Vector and streamline of air flux inside the sample at vacuum pressure of 13.3 kPa and microwave frequency of 5.80 GHz (scale × 30,000,000): (a) t = 10 min, (b) t = 100 min, and (c) t = 360 min.

content inside the sample to decrease. However, at long stages of drying about 180 min, the vapor diffusion effect plays important role in the moisture migration mechanism because of the sustained evaporation that is generated within the sample. The observed moisture profiles in case of vacuum pressure is lower than atmospheric pressure with following reasons. First, at vacuum processing provides the lower boiling point to increase rate of the water evaporation, and so causes moisture to transport upward. Second, vapor flow is greatly improved by increased total pressure gradients, and the effective molecular mass diffusion and binary mass diffusion (as displayed in Eqs. (25) and (26)). Finally, vacuum pressure enhances the mass transfer because of an increased pressure gradient between inside and outside of the sample to be dried.

Fig. 13 shows the microwave power absorbed profile in case of at vacuum pressure of 13.3 kPa and atmospheric pressure, it can be seen that the maximum of microwave power absorbed is occurred for early stage of drying time and is decreased with increasing the elapsed time. As the drying process proceeds, it would eventually cause the average moisture content to decrease and lead to a microwave power absorbed is decreased. The microwave power absorbed is directly affected by dielectric properties as a function of temperature and moisture content. The dielectric loss coefficient is significantly decreased with increasing temperature (further details shown in [35]). Therefore, the microwave power absorbed in case of vacuum pressure is lower than atmospheric pressure because of vacuum pressure corresponding to lower moisture content and higher pressure gradient between inside and outside the sample.

Fig. 14 shows pressure difference profile within the sample at vacuum and atmospheric pressure drying condition. The pressure difference is defined as total gas pressure p_g is subtracted by boundary pressure p_b. It is found that p_b is equal to 13.3 kPa and 101.325 kPa in case of vacuum and atmospheric pressure, respectively. As the drying process proceeds, total pressure is rapidly buildup within the sample and is increasingly contributed by the amount of accumulated vapor owing to the high diffusive vapor flux. It is seen that high temperature and pressure gradient are generated within the sample during particularly the constant rate period. As a result, the capillary action plays an important role in the moisture migration mechanism, and maintains a good supply of liquid to the surface. However, in vacuum pressure drying provides the greater pressure gradient than atmospheric pressure drying, because water evaporation within the sample is accelerated by the higher microwave power absorbed together with the lower boiling point of water.

In order to get more insight into the fluid transport, it is important to investigate the fluid movements within the sample in depth. The vapor, liquid and air flux profiles in case of atmospheric and vacuum pressure at various drying times as 1 of 10, 100 and 360 min are shown in Figs. 15–20, respectively. It can be seen that the vapor flux flows within the sample toward the surface which water evaporation is taken place inside the sample and on the surface. As drying process proceeds, the vapor flux flows throughout the sample migrates in the direction of decreasing saturation. For the liquid flux, it can be observed that almost all of the liquid has migrated toward the upper surface of the sample due to capillary pressure and gas pressure buildup, which are simultaneously changed due to the effect of saturation and temperature distribution in each time period. The air flux moves toward the heated surface with a lower than the vapor flux because the air diffusion is decreased by the convective air flux whereas the vapor diffusion is enhanced by the convective vapor flux. As the rate of liquid supply to the surface becomes lower than the water evaporation rate lead to the void volume is increased; therefore, allowing air flows away from heated surface toward the other surface. The results of all flux profiles in case of vacuum pressure is greater than atmospheric pressure because water evaporation within the sample is accelerated by lower boiling point of water together with higher microwave power absorbed, and higher pressure gradient.

5.3. The effect of microwave frequency

The investigated microwave frequencies are 2.45 and 5.8 GHz in discussion the effect of microwave frequency, which are chosen to show microwave heating phenomena because there are in set of frequencies reserved for industrial, scientific, and medical (ISM band) use. The dielectric properties of water at microwave frequency of 5.8 GHz is refer to Meissner and Wentz [36]. The penetration depth for operating microwave frequencies of 2.45 GHz and 5.8 GHz are 200.11 mm and 52.05 mm, respectively, at initial saturation of S_{in} = 0.6.

Fig. 8(c) shows the electric field distribution inside a rectangular waveguide when the sample is inserted within the waveguide during microwave heating with operating microwave frequency of 2.45 GHz and vacuum pressure of 13.3 kPa. Since the typical depth of sample (50.0 mm) is less than the penetration depth of microwave (200.11 mm), so a large part of microwave is able to penetrate through the sample. The reflected waves occur on each interface, from air (cavity) to upper surface and from lower surface of sample to air (cavity). The reflection and transmission components at each interface contribute to the resonance of standing wave configuration inside the sample and give rise to a microwave

power absorbed peak further from the surface exposed to incident microwaves as seen in Fig. 13(b). Thereafter the microwave power absorbed is converted to the thermal energy and temperature is increased.

Fig. 8(c) presents the electric field distribution inside a rectangular waveguide when the sample is inserted inside the waveguide during microwave heating with the frequency of 2.45 GHz. The penetration of this microwave is higher than the typical depth of sample as seen in Table 2, thus a large part of microwaves are able to penetrate through the sample. The reflected wave occurs on each interface, from air (cavity) to upper surface and from lower surface of sample to air (cavity). The reflection and transmission components at each interface contribute to the resonance of standing wave configuration inside the sample and give rise to a microwave absorption peak further from the surface exposed to incident microwaves. Thereafter the microwave power absorbed is converted to the thermal energy, which increases the sample temperature.

Fig. 21(b) illustrates the electric field distributions inside a rectangular waveguide when the sample is inserted in the waveguide during microwave heating with the microwave frequency of 5.8 GHz. In contrast to the electric field configuration in case of 2.45 GHz, this is a result of a transmitted wave at the incident face and a reflected wave from the lower surface of the sample. This is due to the fact that microwave operating at a high frequency has a short wavelength which corresponds to a smaller penetration depth of microwave as compared with in case of 2.45 GHz (as seen in Table 2) and slightly higher than the depth of sample. Consequently, most microwaves are absorbed by the sample.

Fig. 22 shows the temperature profiles with different z-depths at x-width of 54.61 mm in case of vacuum pressure of 13.3 kPa and microwave frequency of 5.80 GHz. Fig. 23 shows temperature distribution inside the sample at various drying time as 10, 100 and 360 min. Since the higher microwave frequency, 5.8 GHz, has a short wavelength which corresponds to a smaller penetration of microwave. Consequently, most microwaves are absorbed by the sample. Therefore the microwave power absorbed is the greatest at the surface exposed to incident microwave as shown in Fig. 25, and decays exponentially along the propagating direction with a small wavelength. As a result, maximum temperatures are occurred at depth-z of 22.0, 46.0 and 46.0 mm for exposure time of 10, 100 and 360 min, respectively, as shown in Fig. 23. In contrast that to in case of 2.45 GHz illustrated in Fig. 11, maximum temperatures are at the depth-z of 44.0, 48.0 and 48.0 mm for drying time of 10, 100 and 360 min, respectively.

Fig. 24 presents saturation profiles at vacuum pressure of 13.3 kPa and operating microwave frequency of 5.8 GHz. The observed moisture profiles in case of 5.8 GHz are higher than 2.45 GHz because of lower microwave power absorbed.

Fig. 25 shows microwave power absorbed profile within the sample in case of operating microwave frequency of 5.8 GHz. The microwave power absorbed is lower than in case of 2.45 GHz because of a smaller penetration of microwave.

Fig. 26 shows pressure difference profile within the sample in case of operating microwave frequency of 5.8 GHz. Total pressure is lower than in case of 2.45 GHz because it is lower microwave power absorbed profiles taken place inside the sample.

Figs. 27–29 illustrate fluid movement patterns inside the sample in case of microwave frequency of 5.8 GHz at various times as 10, 100 and 360 min. For fluid transport phenomena in terms of liquid, vapor and air flux are explained in previous subsection.

This study shows the capability of the numerical analysis to handle heat-mass transport and pressure buildup in two-dimensional porous medium subjected to a combined microwave and vacuum system. With further quantitative validation of the present method, this method can be used as a tool for investigating in detail this particular microwave drying under vacuum pressure of phase change in an unsaturated porous media at a fundamental level.

6. Conclusions

The numerical analysis presented describes many important interactions within the sample (as an unsaturated porous media) during microwave vacuum drying. A generalized 2D mathematical model for analysis of heat and mass transfer, and pressure buildup in the sample subjected to microwave energy can be used successfully to descript transport phenomena under vacuum pressure condition. The vacuum pressure significant influences to temperature, microwave power absorbed, saturation and pressure buildup distribution, and movement of fluid inside the sample.

Acknowledgments

The authors gratefully acknowledge the Thailand Research Fund (TRF) for supporting this research project.

References

[1] A.S. Mujumdar, Handbook of Industrial Drying, second ed., Marcel Dekker, New York, 1995.
[2] A.C. Metaxas, R.J. Meridith, Industrial Microwave Heating, Peter Peregrinus Ltd., London, 1983.
[3] A.K. Datta, R.C. Anantheswaran, Handbook of Microwave Technology for Food Applications, Marcel Dekker, New York, 2001.
[4] P. Perré, S. Mosnier, I.W. Turner, Vacuum drying of wood with radiative heating. I. Experimental procedure, AIChE J. 50 (2004) 97–107.
[5] W. Jomaa, O. Baixeras, Discontinuous vacuum drying of oak wood: modelling and experimental investigations, Drying Technol. 15 (9) (1997) 2129–2144.
[6] A.E. Drouzas, H. Schubert, Microwave application in vacuum drying of fruits, J. Food Eng. 28 (1996) 203–209.
[7] A.E. Drouzas, E. Tsami, G.D. Saravacos, Microwave/vacuum drying of model fruit gels, J. Food Eng. 39 (1999) 117–122.
[8] C. Péré, E. Rodier, Microwave vacuum drying of porous media: experimental study and qualitative considerations of internal transfers, Chem. Eng. Process. 41 (2002) 427–436.
[9] P.S. Sunjka, T.J. Rennie, C. Beaudry, G.S.V. Raghavan, Microwave-convective and microwave-vacuum drying of cranberries: a comparative study, Drying Technol. 22 (5) (2004) 1217–1231.
[10] Q. Hu, M. Zhang, A.S. Mujumdar, G. Xiao, J. Sun, Drying of edamames by hot air and vacuum microwave combination, J. Food Eng. 77 (2006) 977–982.
[11] P. Perré, I.W. Turner, A 3-D version of TransPore: a comprehensive heat and mass transfer computational model for simulating the drying of porous media, Int. J. Heat Mass Transfer 42 (1999) 4501–4521.
[12] P. Rattanadecho, W. Pakdee, J. Stakulcharoen, Analysis of multiphase flow and heat transfer: pressure buildup in an unsaturated porous slab exposed to hot gas, Drying Technol. 26 (2008) 39–53.
[13] H. Ni, A.K. Datta, K.E. Torrance, Moisture transport in intensive microwave heating of biomaterials: a multiphase porous media model, Int. J. Heat Mass Transfer 42 (1999) 1501–1512.
[14] P. Ratanadecho, K. Aoki, M. Akahori, A numerical and experimental investigation of the modeling of microwave drying using a rectangular wave guide, Drying Technol. 19 (9) (2001) 2209–2234.
[15] L.A. Campañone, N.E. Zaritzky, Mathematical analysis of microwave heating process, J. Food Eng. 69 (3) (2005) 359–368.
[16] W. Cha-um, P. Rattanadecho, W. Pakdee, Experimental analysis of microwave heating of dielectric materials using a rectangular waveguide (MODE: TE10) (case study: water layer and saturated porous medium), Exp. Therm. Fluid Sci. 33 (3) (2009) 472–481.
[17] P. Rattanadecho, N. Suwannapum, W. Cha-um, Interactions between electromagnetic and thermal fields in microwave heating of hardened type I-cement paste using a rectangular waveguide (influence of frequency and sample size), ASME J. Heat Transfer 131 (2009) 082101–082112.
[18] L. Hansson, L. Antti, Modeling microwave heating and moisture redistribution in wood, Drying Technol. 26 (2010) 552–559.
[19] D. Jia, M.T. Afzal, Modeling the heat and mass transfer in microwave drying of white oak, Drying Technol. 26 (2008) 1103–1111.
[20] S. Sungsoontorn, P. Rattanadecho, W. Pakdee, One-dimensional model of heat and mass transports and pressure buildup in unsaturated porous materials subjected to microwave energy, Drying Technol. 29 (2011) 189–204.
[21] N. Suwannapum, P. Rattanadecho, Analysis of heat–mass transport and pressure buildup induced inside unsaturated porous media subjected to microwave energy using a single (TE10) mode cavity, Drying Technol. 29 (2011) 1010–1024.

[22] P. Ratanadecho, K. Aoki, M. Akahori, A numerical and experimental investigation of the modeling of microwave heating for liquid layers using a rectangular waveguide (effects of natural convection and dielectric properties), Appl. Math. Model. 26 (3) (2002) 449–472.
[23] S. Tada, R. Echigo, Y. Kuno, H. Yoshida, Numerical Analysis of Electromagnetic Wave in Partially Loaded Microwave Applicator, Int. J. Heat Mass Transfer 41 (1998) 709–718.
[24] J. Wang, T. Schmugge, An empirical model for the complex dielectric permittivity of soil as a function of water content, IEEE Trans. Geosci. Remote Sens. GE-18 (4) (1980) 288–295.
[25] T. Basak, K. Aparna, A. Meenakshi, A.R. Balakrishnan, Effect of ceramic supports on microwave processing of porous food samples, Int. J. Heat Mass Transfer 49 (2006) 4325–4339.
[26] P. Ratanadecho, K. Aoki, M. Akahori, Influence of irradiation time, particle sizes, and initial moisture content during microwave drying of multi-layered capillary porous materials, ASME J. Heat Transfer 124 (2002) 151–161.
[27] G. Mur, Absorbing boundary conditions for the finite-difference approximation of the time-domain electromagnetic-field equations, IEEE Trans. Electromagn. Compat. EMC-23 (4) (1981) 377–382.
[28] S. Whitaker, A theory of drying in porous media, Adv. Heat Transfer 13 (1977) 119–203.
[29] M. Kaviany, Principle of Heat Transfer in Porous Media, Springer, New York, 1991.
[30] M. Kaviany, M. Mittal, Funicular state in drying of porous slab, Int. J. Heat Mass Transfer 30 (7) (1987) 1407–1418.
[31] K. Aoki, M. Hattori, M. Kitamura, N. Shiraishi, Characteristics of heat transport in porous media with water infiltration, ASME/JSME Therm. Eng. Proc. 4 (1991) 303–308.
[32] J.A. Rogers, M. Kaviany, Funicular and evaporative-front regimes in convective drying of granular beds, Int. J. Heat Mass Transfer 35 (1992) 469–479.
[33] J. Watanuki, Fundamental study of microwave heating with rectangular wave guide, M.S. Thesis, Nagaoka University of Technology, Japan, 1998, p. 85.
[34] V. Changrue, Hybrid (osmotic, microwave-vacuum) drying of strawberries and carrots, Ph.D. Thesis, Macdonald Campus of McGill University, Canada, 2006.
[35] P. Ratanadecho, K. Aoki, M. Akahori, Experimental and numerical study of microwave drying in unsaturated porous material, Int. Commun. Heat Mass Transfer 28 (2001) 605–616.
[36] T. Meissner, F.J. Wentz, The complex dielectric constant of pure and sea water from microwave satellite observations, IEEE Trans. Geosci. Remote Sens. 42 (9) (2004) 1836–1849.